The Cryosphere, 12, 1899–1919, 2018
https://doi.org/10.5194/tc-12-1899-2018

The Cryosphere Open Access EGU

Multi-decadal mass balance series of three Kyrgyz glaciers inferred from modelling constrained with repeated snow line observations

Martina Barandun[1], Matthias Huss[1,2], Ryskul Usubaliev[3], Erlan Azisov[3], Etienne Berthier[4], Andreas Kääb[5], Tobias Bolch[6], and Martin Hoelzle[1]

[1]Department of Geosciences, University of Fribourg, Fribourg, Switzerland
[2]Laboratory of Hydraulics, Hydrology and Glaciology (VAW), ETH Zurich, Zurich, Switzerland
[3]Central Asian Institute of Applied Geosciences (CAIAG), Bishkek, Kyrgyzstan
[4]CNRS, LEGOS, University of Toulouse, Toulouse, France
[5]Department of Geosciences, University of Oslo, Oslo, Norway
[6]Department of Geography, University of Zurich, Zurich, Switzerland

Correspondence: Martina Barandun (martina.barandun@unifr.ch)

Received: 15 November 2017 – Discussion started: 27 November 2017
Revised: 22 March 2018 – Accepted: 3 April 2018 – Published: 6 June 2018

Abstract. Glacier surface mass balance observations in the Tien Shan and Pamir are relatively sparse and often discontinuous. Nevertheless, glaciers are one of the most important components of the high-mountain cryosphere in the region as they strongly influence water availability in the arid, continental and intensely populated downstream areas. This study provides reliable and continuous surface mass balance series for selected glaciers located in the Tien Shan and Pamir-Alay. By cross-validating the results of three independent methods, we reconstructed the mass balance of the three benchmark glaciers, Abramov, Golubin and Glacier no. 354 for the past 2 decades. By applying different approaches, it was possible to compensate for the limitations and shortcomings of each individual method. This study proposes the use of transient snow line observations throughout the melt season obtained from satellite optical imagery and terrestrial automatic cameras. By combining modelling with remotely acquired information on summer snow depletion, it was possible to infer glacier mass changes for unmeasured years. The model is initialized with daily temperature and precipitation data collected at automatic weather stations in the vicinity of the glacier or with adjusted data from climate reanalysis products. Multi-annual mass changes based on high-resolution digital elevation models and in situ glaciological surveys were used to validate the results for the investigated glaciers. Substantial surface mass loss was confirmed for the three studied glaciers by all three methods, ranging from -0.30 ± 0.19 to -0.41 ± 0.33 m w.e. yr^{-1} over the 2004–2016 period. Our results indicate that integration of snow line observations into mass balance modelling significantly narrows the uncertainty ranges of the estimates. Hence, this highlights the potential of the methodology for application to unmonitored glaciers at larger scales for which no direct measurements are available.

1 Introduction

Glaciers are important components of the hydrological cycle in central Asia. In this arid continental region, the intensely populated and irrigated downstream areas strongly depend on a supply of water from the cryosphere such as glaciers and snow (Kaser et al., 2010; Schaner et al., 2012; Duethmann et al., 2014; Chen et al., 2016; Huss and Hock, 2018). The uncertainty of water availability in the context of a changing climate creates a major potential for political tension and builds a complex set of future threats, affecting different sectors such as water management, energy production and irrigation (Varis, 2014; Munia et al., 2016). Climate change poses a manifold challenge for the central Asian population and will influence natural hazards and threaten future economies and the livelihoods of coming generations (Stocker et al., 2013). For this reason, continuous and high-quality data for the different components of the hydrologi-

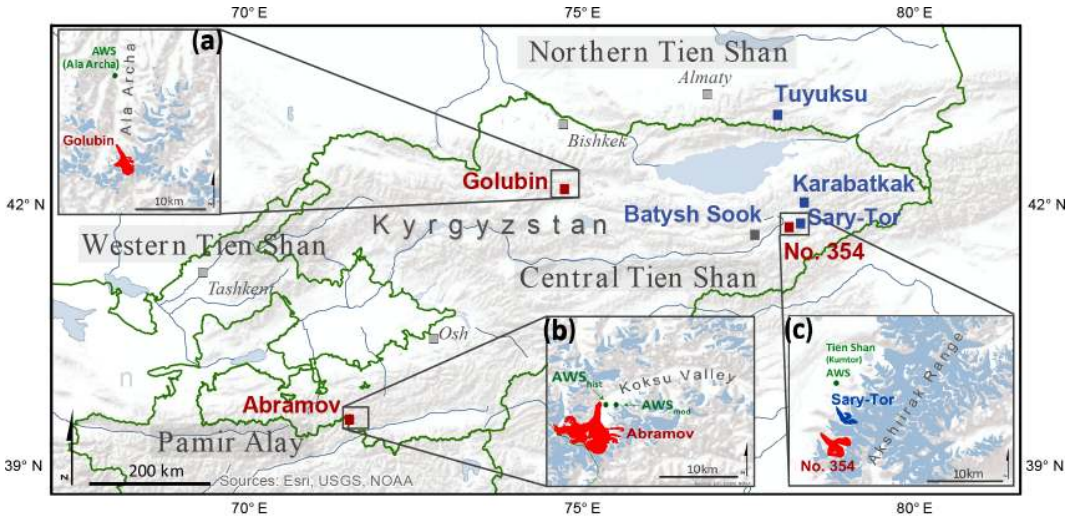

Figure 1. Overview map of central Asia showing the location of glaciers (blue) with available long-term SMB measurements. Glaciers investigated in this study are marked in red. The insets show the position of the automatic weather station (AWS) for **(a)** Golubin, **(b)** Abramov and **(c)** Glacier no. 354. Note that AWS_{mod} indicates the position of the new AWS installed in 2011 and AWS_{hist} the old glaciological station at Abramov.

cal cycle acquired within established regional and national cryospheric and hydrologic climate services are key for providing accurate predictions which enable sustainable adaptation. As stated by the World Meteorological Organization (GCOS, 2016), large gaps currently exist in the global climate observation system. This refers in equal measure to remote and unmonitored areas, especially in the Pamir, but also in the Tien Shan, where there is a lack of data that is crucially needed to plan and enhance future development (Sorg et al., 2012; Unger-Shayesteh et al., 2013). Improved temporal and spatial representation of glacier monitoring is thus essential, due to the paramount significance of glaciers in the high-mountain cryosphere.

During the Soviet era, in the 1950s and 1960s, an extensive system of cryospheric monitoring was launched in the Tien Shan and Pamir-Alay. Most programmes stopped abruptly after the breakdown of the USSR in the mid-1990s. Monitoring activities were maintained only on Tuyuksu Glacier, Kazakhstan and Urumqi Glacier (no. 1), China. In recent years, different initiatives have aimed at the re-establishment of glacier monitoring in central Asia (Hoelzle et al., 2017). Surface mass balance (SMB) series are now available for the following glaciers: Abramov (Pamir-Alay), Batysh Sook, Sary-Tor, Karabatkak and Glacier no. 354 (central Tien Shan), for Urumqi no. 1 (eastern Tien Shan) and Golubin and Tuyuksu (northern Tien Shan) (Fig. 1) (WGMS, 2013). However, a significant gap in the data from the mid-1990s to around 2010 hinders the interpretation of long-term trends in glacier behaviour in this region.

Different studies derived continuous mass balance series for selected glaciers based on modelling (e.g. Fujita et al., 2011; Barandun et al., 2015; Kronenberg et al., 2016; Liu and Liu, 2016; Kenzhebaev et al., 2017) and estimated mass balance at a regional scale in the Pamir-Alay and Tien Shan (Farinotti et al., 2015). Modelled mass balance series have good temporal resolution; however, they are not observation-based and thus strongly depend on model calibration and the quality of the input variables. Several studies use remote sensing techniques to fill the gaps in glacier monitoring and to generate insights into region-wide mass changes covering the entire High Mountain Asia within the past 2 decades (e.g. Gardner et al., 2013; Gardelle et al., 2013; Kääb et al., 2015; Brun et al., 2017; Wang et al., 2017). Furthermore, other authors focused on selected regions of the central and northern Tien Shan (e.g. Aizen et al., 2007; Pieczonka et al., 2013; Bolch, 2015; Pieczonka and Bolch, 2015; Goerlich et al., 2017), deriving glacier-specific geodetic mass balances. These studies often cover large areas, but temporal resolution is typically limited to 5 years or longer periods. Thus, they fail to capture the interannual or even seasonal signals.

The snow line is recognized as a valuable proxy for glacier mass balance (LaChapelle, 1962; Lliboutry, 1965; Braithwaite, 1984; Kulkarni, 2012; Rabatel et al., 2017). Different methods have been developed to use the end-of-summer snow line observed on air- and space-borne data, i.e. without direct access to the glacier, to infer glacier mass changes based on a statistical relation between the equilibrium line altitude and the glacier-wide SMB (e.g. Kulkarni, 1992; Dyurgerov, 1996; Rabatel et al., 2005). These methods were applied to glaciers located in a wide range of different regions, such as in Europe (e.g. Hock et al., 2007; Rabatel et al., 2008, 2016), South America (e.g. Rabatel et al., 2012), New Zealand (e.g. Chinn, 1995, 1999), the Arctic (e.g.

Table 1. Available data on glacier monitoring for the three glaciers used in this study. The dates marked with an asterisk indicate the DEMs used as a topographic base for the modelling.

	Abramov	Golubin	Glacier no. 354
No. of surface mass balance measurements per year	22	14	16
No. of annual glaciological surveys (2000–2016)	5	6	6
Total no. of snow line observations	122	56	78
High-resolution satellite stereo images	27 Aug 2003 (SPOT5)	8 Sep 2006 (ALOS)*	1 Sep 2003 (QuickBird)
	29 Nov 2011 (SPOT5)	1 Nov 2014 (SPOT7)	27 Jul 2012 (GeoEye)*
	1 Sep 2015 (Pléiades)*		1 Oct 2015 (SPOT6)

Mernild et al., 2013), the Himalayas (e.g. Kulkarni et al., 2004, 2011) and central Asia (e.g. Dyurgerov et al., 1994; Kamniansky and Pertziger, 1996). Some pioneer studies (e.g. Østrem, 1973, 1975; Young, 1981; Dyurgerov et al., 1994) have identified the value of transient snow line (TSL) observations in connection with subseasonal SMB. Recent studies (e.g. Hock et al., 2007; Pelto, 2010; Pelto et al., 2013; Huss et al., 2013; Hulth et al., 2013) have further developed this concept to improve surface mass balance monitoring and modelling strategies, including information extracted from continuous TSL observations. However, most approaches still rely on long-term glaciological information and are thus not applicable to unmonitored glaciers located in remote and unmeasured regions.

In this study, three pillars of a multi-level strategy for glacier observation are combined, covering the period of the past 2 decades, to improve the understanding of mass change evolution of Abramov, Golubin and Glacier no. 354, three benchmark glaciers in the Tien Shan and Pamir-Alay. (1) We integrate in situ glaciological measurements, when available, to compute annual SMB using a model-based extrapolation of the measurement points to reach glacier-wide coverage. (2) We calculate geodetic mass changes based on high-resolution digital elevation models (DEMs) on decadal to semi-decadal timescales. (3) We infer daily SMB series using a model approach supported by TSL observations, as a proxy for glacier mass balance. In this way, a temperature-index model is calibrated with the snow-covered area fraction (SCAF) of the glacier observed on satellite optical imagery and time-lapse photographs throughout the ablation season. This approach represents a new tool for glacier observation at high temporal and spatial resolution. The remote snow line observations provide valuable information, especially for periods for which no direct measurements are available. By combining different independent approaches, we aim to overcome the limitations and shortcomings of each individual method and to deliver a robust mass balance estimate for the three selected glaciers at annual resolution for a period for which only limited data have been available so far.

2 Study sites and data

2.1 Study sites

In this section we present a brief overview of the study sites. A detailed description of the three selected glaciers and their geographic and climatological settings is given in Hoelzle et al. (2017). Table 1 summarizes the available data for each glacier.

2.1.1 Abramov Glacier

Abramov Glacier (39°36.78′ N, 71°33.32′ E) is located in the Pamir-Alay (north-western Pamir, Fig. 1). The north- to north-east-facing glacier has an extent of about 24 km^2 (as of 2016) and ranges from 3650 to nearly 5000 m a.s.l. Barandun et al. (2015) suggested that the glacier had a mean annual balance of -0.44 ± 0.10 m w.e. yr^{-1} between 1968 and 2014 and estimated internal accumulation and basal ablation to contribute $+0.07$ m w.e. yr^{-1} to the total mass change of the glacier. Brun et al. (2017) indicated a mass loss of -0.38 ± 0.10 m w.e. yr^{-1} for Abramov from ca. 2002 to 2014.

Mean daily air temperature and total daily precipitation sums were measured at a glaciological station located at 3837 m a.s.l. from 1967 to 1998 (Fig. 1). The station was located at a distance of about 0.5 km from the glacier tongue. Air temperature measured at an automatic weather station (AWS_{mod}) was used from 2011 to 2016 (Fig. 2a). This station is located at an elevation of 4100 m a.s.l. at a distance of about 1.5 km from the glacier terminus. ERA-Interim reanalysis data with a spatial resolution of 0.78° (Dee et al., 2011) were used to fill measurement gaps (Barandun et al., 2015).

The SMB was measured intensively from 1967 to 1998 (Suslov et al., 1980; Glazirin et al., 1993) and the monitoring was re-established in 2011 (Hoelzle et al., 2017). Since then, annual glaciological surveys were continuously carried out in late August. For a reanalysed and reconstructed mass balance series for Abramov from 1968 to 2014 and a detailed description of the measurement network see Barandun et al. (2015).

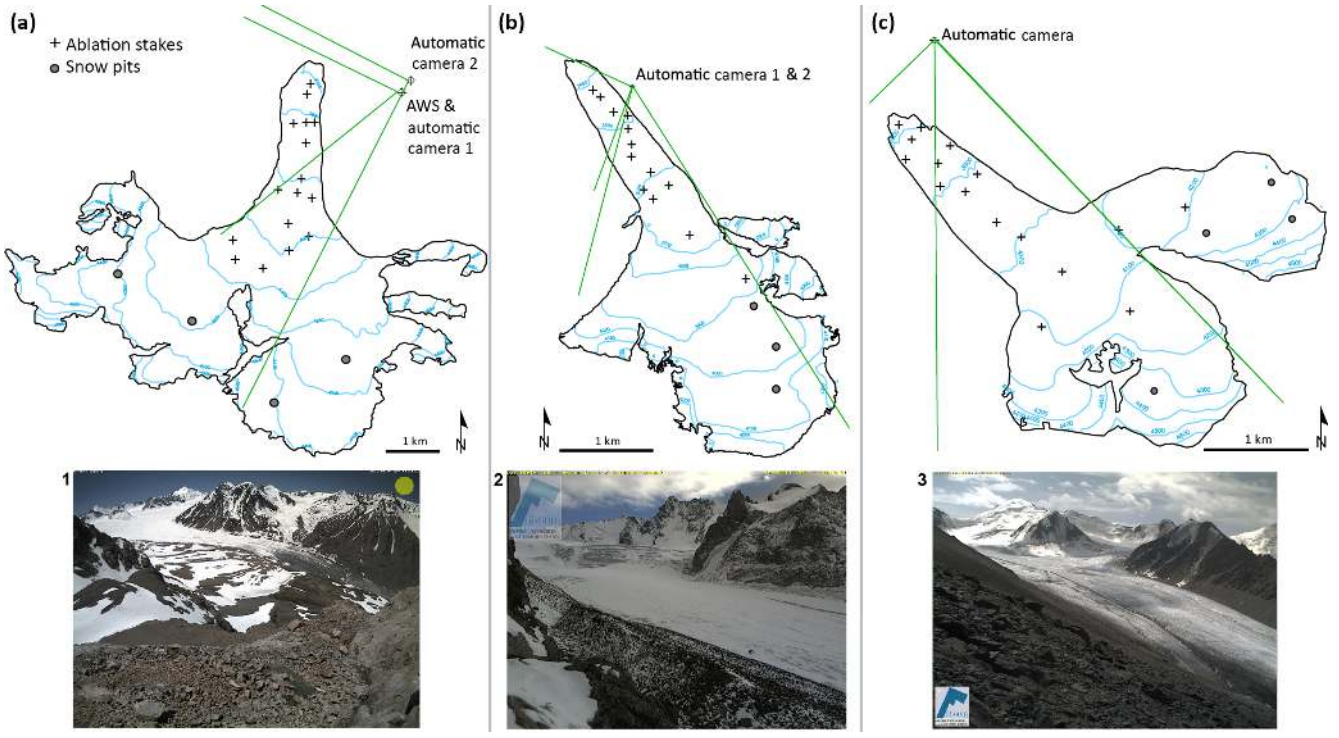

Figure 2. Glacier monitoring network at **(a)** Abramov, **(b)** Golubin and **(c)** Glacier no. 354. A photograph taken by the terrestrial cameras is shown for **(1)** Abramov, **(2)** Golubin and **(3)** Glacier no. 354.

2.1.2 Golubin Glacier

Golubin Glacier (42°26.94′ N, 74°30.10′ E) is located in the Ala Archa Valley in the Kyrgyz Ala-Too mountains in the northern Tien Shan (Fig. 1). The glacier has an area of $\sim 5\,\mathrm{km}^2$ (as of 2016) and a north to north-western aspect. The terminus is currently located at an elevation of about 3400 m a.s.l. and the glacier extends to an elevation of about 4300 m a.s.l. Long-term measurements indicated an internal accumulation due to the refreezing of meltwater of about $+0.08\,\mathrm{m\,w.e.\,yr}^{-1}$ (Aizen et al., 1997). For Golubin, the geodetic mass loss reported by Bolch (2015) was $-0.28 \pm 0.96\,\mathrm{m\,w.e.\,yr}^{-1}$ from ~ 2000 to 2012, whereas Brun et al. (2017) found a geodetic mass balance of $-0.04 \pm 0.19\,\mathrm{m\,w.e.\,yr}^{-1}$ for the period 2002 to 2013.

We used meteorological data from the Alplager station located in the Ala Archa Valley, situated at an elevation of 2145 m a.s.l. at a distance of about 10 km from the glacier (Fig. 1). There are several other meteorological stations in the valley; however, the Alplager station has the most complete and continuous series at high elevation, covering the entire study period.

Intense glacier monitoring started in 1958 and continued until 1994 (Aizen, 1988). In summer 2010, SMB measurements were re-initiated. Figure 2b summarizes the monitoring network at Golubin as of 2016, including a SMB measurement network, an AWS (≈ 3300 m a.s.l.) and two terrestrial cameras installed in 2013. A detailed description of the monitoring strategy is provided in Hoelzle et al. (2017).

2.1.3 Glacier no. 354

Glacier no. 354 (41°47.62′ N, 78°9.69′ E) is situated in the Ak-shiirak range in the central Tien Shan (Fig. 1). The glacier covered a surface area of about $6.4\,\mathrm{km}^2$ in 2016. The accumulation zone comprises three basins and the glacier tongue is oriented to the north-west. The glacier spans an elevation range of 3750–4680 m a.s.l. Mass loss since the mid-1970s was reported by different studies to range from about -0.8 to $-0.5\,\mathrm{m\,w.e.\,yr}^{-1}$ (Pieczonka and Bolch, 2015; Kronenberg et al., 2016; Brun et al., 2017). Summer snowfall is frequent and fresh snow can cover the entire glacier surface for several days during the melt season, significantly reducing ablation (Kronenberg et al., 2016). Evidence of persistent superimposed ice is found and Kronenberg et al. (2016) estimated internal accumulation to be $+0.04\,\mathrm{m\,w.e.\,yr}^{-1}$. An AWS (Tien Shan, Kumtor AWS) installed at an elevation of ≈ 3660 m a.s.l. and a distance of approximately 10 km to the glacier recorded continuous meteorological data for the study period (Fig. 1). We used daily precipitation sums and mean daily air temperature for the modelling.

Since 2010, in situ SMB has been obtained annually in late summer (Fig. 2c). Winter measurements exist for May 2014 (Kronenberg et al., 2016). A description of the meteorologi-

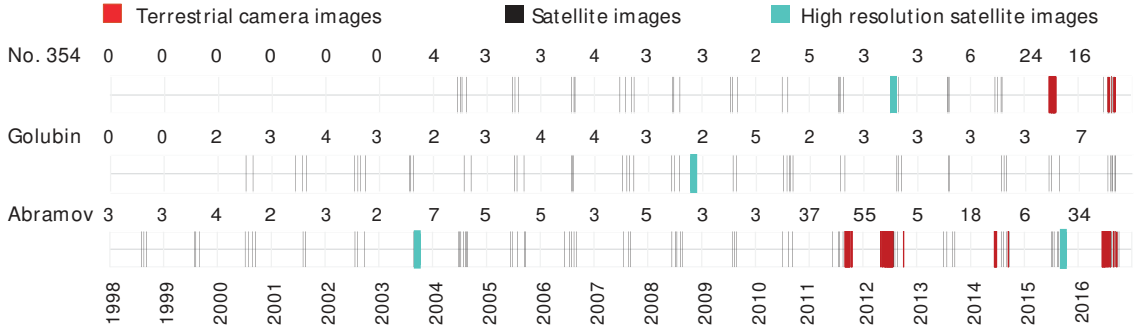

Figure 3. Image availability and distribution for snow line mapping. Numbers indicate the total available scenes per year and glacier. Prior to 1998, image coverage is sparse for all three glaciers. For Golubin and Glacier no. 354, the first summer seasons for which enough TSL observations could be collected were in 2000 and 2004, respectively. Snow-covered high-resolution images have not been used to delineate the snow line and are not shown here.

cal input data and the SMB measurement network as well as a reconstruction of the mass balance series back to 2003 are provided by Kronenberg et al. (2016).

2.2 High-resolution satellite images and DEMs

To compute geodetic mass balances for Abramov, high-resolution DEMs were used based on Pléiades stereo images acquired in 2015 and on stereo images from 2003 and 2011 from Satellite Pour l'Observation de la Terre (SPOT) 5. For Glacier no. 354, DEMs from 2003 (QuickBird) and 2012 (GeoEye) were available from Kronenberg et al. (2016). In addition, a SPOT6 stereo-pair acquired in 2015 was used to produce an updated DEM. High-resolution stereo images for Golubin are sparse and we had to rely on a SPOT7 tri-stereo scene from November 2014 and on Advanced Land Observing Satellite (ALOS) Prism scenes from 2006 (Table 1). Significant snow coverage was present on the SPOT5 image from 2011 for Abramov and on the SPOT7 image from 2014 for Golubin. A fine layer of fresh snow covered parts of the SPOT6 image from 2015 for Glacier no. 354. For modelling purposes, the most complete and accurate DEM available for each glacier was used to represent the surface topography (Table 1).

2.3 Optical satellite and terrestrial camera images

We used freely accessible, orthorectified and georeferenced Landsat TM/ETM+ and OLI, Terra ASTER-L1B and Sentinel-2A scenes to repeatedly observe the glacier outlines and the TSL throughout the melt season for all three glaciers. In addition, we used the snow-free high-resolution optical satellite images as described above for TSL and glacier outline mapping.

Two terrestrial cameras (Mobotix M25) overlooking Abramov were installed in August 2011. One camera was located next to the AWS_{mod} and the other one at approximately 500 m distance at an elevation of 4200 m a.s.l. (Fig. 2a). Due to multiple camera failures and power supply problems, pictures were lacking from the end of the ablation season in 2012 to the end of the ablation season in 2013 and again partly for the summer months in 2014. In 2015, continuous coverage was obtained from Camera 1 but only a few images could be retrieved from Camera 2. A complete set of data was collected from both cameras for the first time in 2016. A similar set-up has been installed for Glacier no. 354 in 2014, delivering continuous coverage since implementation (Fig. 2c). The camera is located at an elevation of 4145 m a.s.l. Images from the two cameras installed at Golubin were not used here due to limited image quality (Fig. 2b). Figure 3 illustrates the number of camera and satellite images with satisfying quality that were used to obtain maps of snow lines for the three glaciers. Image availability for TSL mapping prior to 1998 was insufficient for the most part.

3 Methods

3.1 Glacier outlines

Glacier extents were mapped manually based on satellite images for all three glaciers and for each year of the corresponding study period. Only cloud- and snow-free images were selected. The surfaces of Glacier no. 354 and Golubin are mostly debris-free. We excluded a debris-covered part with strongly reduced melt rates at the western margin of Abramov (Barandun et al., 2015). Annually repeated measurements of the glacier front position using a handheld GPS for all three glaciers were combined with the satellite observations for mapping from 2011 onward. The same outlines were used for all three methods. Errors related to glacier outlines digitized manually on remote sensing images depend on atmospheric and topographic corrections, shading, glacier surface characteristics, snow cover and local clouds, but mainly on the misinterpretation of debris cover (Paul et al., 2013, 2015). Uncertainties are expected to be

in the range of $\pm 5\,\%$ of the total glacier area for medium-resolution images such as Landsat TM and are smaller for high-resolution images (Paul et al., 2013).

3.2 Meteorological data

For Abramov, the air temperature data measured at the AWS were adjusted to the elevation of the former glaciological station by applying a constant lapse rate of $-6\,^{\circ}\mathrm{C\,km^{-1}}$ (Suslov et al., 1980). The ERA-Interim reanalysis data set was adapted by applying mean monthly additive and multiplicative biases for air temperature and precipitation, respectively. The biases were calculated from long-term in situ measurements (Barandun et al., 2015). From the corrected monthly means, daily series were generated by superimposing day-to-day variability observed at the meteorological station from 1969 to 1994. For Abramov, we generated air temperature series from 1995 to 2011 and precipitation series from 1995 to 2016. More detailed information on data preparation and their suitability is given in Barandun et al. (2015).

Mean daily air temperature data measured at the Ala Archa AWS and Tien Shan (Kumtor) AWS were extrapolated to the median elevation of the corresponding glacier with monthly temperature lapse rates for the northern and central Tien Shan provided in Aizen et al. (1995).

3.3 Snow line delineation

A visual preselection of suitable camera and satellite images was taken in order to preclude problems associated with image quality such as fresh snowfall and extensive cloud cover. Oblique ground-based photographs were first corrected automatically for lens distortion, then projected and orthorectified following Corripio (2004). Every pixel on the photograph was associated with the elevation of the DEM. Georeferenced products of satellite scenes were downloaded. On each camera and satellite image, the snow-covered area was digitized manually by means of visual separation of bare ice and snow (Pelto et al., 2013; Mernild et al., 2013; Huss et al., 2013). Manual detection allowed the observer's knowledge of the snow cover depletion patterns to be integrated and was assumed to be less error-prone than an automatic classification (Huss et al., 2013; Rabatel et al., 2013).

Errors occurred due to the pixel size of the images, slope of the terrain, the accuracy of the georeferencing and the quality of the DEM (Rabatel et al., 2012). In view of the fact that the border between ice and snow is not a clearly defined line, operator expertise is desired and beneficial. The contrast becomes rather weak, especially when the snow line rises above the firn line (Rabatel et al., 2013; Wu et al., 2014) for both satellite and terrestrial camera images. In order to estimate the influence of ambiguous transition areas, we conducted extensive experiments on the interpretation of the surface type (see Sect. 4).

We assumed the spatial depletion pattern to be approximately constant in time so that camera and satellite images with minor invisible sections of the snow line due to shading, cloud cover, Landsat 7 SLC-off void-stripes or the terrestrial camera viewing angle could be included. To fill in those data gaps, we extrapolated the snow line based on information from repeated TSL observations of images with good quality over a $\approx$ 15-year period. The effect of a misinterpretation of the snow line on the calculated SMB was investigated in detail and is described in Sect. 4.

3.4 Glaciological surface mass balance

Ablation stakes are distributed over the entire ablation zone in order to provide an optimal representation of melt patterns (Fig. 2). Each year, they are redrilled at the initial position. An ice density of $900\,\mathrm{kg\,m^{-3}}$ was assigned. Snow pits were dug to the previous end-of-summer horizon to measure snow density and snow accumulation. Annual field surveys ranged from late July to late August and, for logistic reasons, can vary from year to year. Winter snow measurements were carried out to retrieve a detailed snow distribution pattern and to compute the winter balance for Glacier no. 354 and Golubin in May 2014 (Kronenberg et al., 2016). Winter surveys from 1993 and 1994 were available for Abramov (Pertziger, 1996). A model-based spatial extrapolation of point measurements to the entire glacier surface after Huss et al. (2009) was used to retrieve glacier-wide SMB for all years with direct measurements. The model is a combined distributed accumulation (Huss et al., 2008) and temperature-index melt model with daily resolution (Hock, 1999) which was automatically optimized to best represent all collected point data from each seasonal and annual survey. The model is considered a suitable tool for extrapolating the glaciological point measurements to the glacier surface for the measurement periods.

3.5 Geodetic mass balance

For Abramov, the 4 m Pléiades DEM from 1 September 2015 was used as a reference. It was created using the AMES stereo-pipeline (Shean et al., 2016) and the processing parameters that were used in Marti et al. (2016). The two SPOT5 DEMs (August 2003 and November 2011) were derived from High Resolution Stereoscopic (HRS) images by the French mapping agency (Korona et al., 2009). The steps required to adjust the two SPOT5 DEMs horizontally and vertically to the Pléiades reference DEM are similar to the ones followed in a previous study on the Mont Blanc area (Berthier et al., 2014).

We created DEMs with a spatial resolution of 5 m for Golubin and Glacier no. 354 from the available stereo and tri-stereo pairs of high-resolution satellite imagery using standard procedures and the software PCI Geomatica (Kronenberg et al., 2016). The stereo and tri-stereo pairs were connected using common tie points before DEM extraction. For

Glacier no. 354, a horizontal shift between the two DEMs was corrected through a DEM co-registration procedure proposed by Nuth and Kääb (2011). For the data covering Golubin, no horizontal shift was encountered. We thus corrected only for a mean elevation difference of 3.9 m detected over stable ground. For this vertical co-registration, only terrain sections with a slope smaller than 30° were selected and areas with parallax-matching problems were avoided. Snow-covered areas were included in the offset correction in order to correct for fresh snow on the image, assuming similar snow thicknesses on- and off-glacier. The vertical accuracy was thus improved, and the mean absolute difference off-glacier was limited to 1.0 m (2003–2015) and 0.6 m (2011–2015) for Abramov, 0.7 m for Glacier no. 354 and 1.6 m for Golubin (see also Section 4). Steep mountain walls and shading caused problems. Areas affected were manually masked out. Unmeasured areas (Abramov: 26 % in 2003–2015 and 23 % in 2011–2015; Golubin: 30%; Glacier no. 354: 25 %) were assumed to have experienced the same elevation change as the measured areas in the same altitude band and the median of the corresponding elevation bin was used for gap-filling. For elevation bins higher than 4300 m a.s.l. at Golubin (9 % of total area) and for elevation bins higher than 4500 m a.s.l. at Glacier no. 354 (8 % of total area), obvious DEM errors were dominant and not enough realistic values for median elevation-change calculation were available. Thus, the median of the uppermost elevation band with reliable data was used to fill in the gaps. To derive the geodetic mass balance ΔM_{geod}, a density $\rho_{\Delta V}$ of 850 kg m^{-3} was used for volume-to-mass conversion (Huss, 2013):

$$\Delta M_{\mathrm{geod}} = \frac{\Delta V \cdot \rho_{\Delta V}}{\overline{A} \cdot \Delta t}, \tag{1}$$

where $\overline{A}$ is the average glacier area and Δt is the time in years between the corresponding image pairs. Uncertainties in the detected elevation changes and the derived geodetic mass balances are described in Sect. 4.

3.6 Surface mass balance modelling constrained by TSL observations

An accumulation and temperature-index melt model closely constrained by TSL observations was implemented in order to infer glacier-wide SMBs. The applied methodology is a further stage in the approach presented by Huss et al. (2013). The principle of the approach is to employ the information given by the temporal change in the position of the TSL throughout the ablation season to constrain both the amount of winter snow accumulation and melt by iteratively calibrating a mass balance model. The approach also allows us to temporally extend SMB estimates to the end of the hydrological year even though snow line observations do not cover the entire ablation season. The methodological steps are described in more detail in the following.

A surface mass balance model with a spatial resolution of 20 m was driven with daily mean air temperature and precipitation sums measured at nearby meteorological stations or inferred from reanalysis data (see Sect. 2.1). We used a classical temperature-index melt model (e.g. Braithwaite, 1995; Hock, 2003). Melt M was calculated for each grid cell x, y and time step t based on a linear relation with positive daily mean air temperature $T_{\mathrm{air}}(x, y, t)$ as

$$M_{x,y,t} = \begin{cases} \mathrm{DDF}_{\mathrm{ice/snow}} \cdot T_{\mathrm{air}(x,y,t)} & T_{\mathrm{air}} > 0^{\circ} \\ 0 & T_{\mathrm{air}} \leq 0^{\circ} \end{cases}. \tag{2}$$

Daily air temperatures are extrapolated to each grid cell using a constant temperature lapse rate based on literature values (Table 3). Different degree-day factors, $\mathrm{DDF}_{\mathrm{ice/snow}}$, were chosen for snow and ice surfaces. The surface type over the glacier area was given by the snow depth updated with modelled daily snowfall and melt. The ratio between $\mathrm{DDF}_{\mathrm{ice}}$ and $\mathrm{DDF}_{\mathrm{snow}}$, R_{DDF}, was held constant over time. As a wide range of different ratios can be found in the literature (e.g. Hock, 2003; Zhang et al., 2006; Gao et al., 2010; Liu and Liu, 2016), we decided to constrain R_{DDF} with SMB measurements in the Tien Shan and Pamir (Table 3). A sensitivity test shows that a variation in R_{DDF} by ±25 %, a value exceeding the maximum range found in the literature (±22 %), only causes small changes in modelled SMB (Table 4) indicating that calibrating R_{DDF} improves model performance to some extent but is not essential when applying the model. For more details see Sect. 4.

Snow accumulation C was calculated for each grid cell x, y and time step t by

$$C_{(x,y,t)} = P_{\mathrm{ws}(x,y,t)} \cdot C_{\mathrm{prec}} \cdot \left(1 + \left(z_{(x,y)} - z_{\mathrm{ws}}\right) \cdot \delta P / \delta z\right), \tag{3}$$

where P_{ws} is the measured precipitation at the meteorological station at elevation z_{ws}. $z_{(x,y)}$ is the elevation of each grid cell. The measured precipitation was extrapolated to every grid cell with a constant precipitation gradient $\delta P / \delta z$ calculated from winter snow surveys (Table 3). Solid precipitation occurs at $T_{\mathrm{air}} \leq 1.5$ °C with a linear transition range of ±1 °C (e.g. Hock, 1999). C_{prec} is a scaling factor that accounts for gauge under-catch and other systematic measurement errors of precipitation (e.g. Huss et al., 2009). In order to account for smaller measurement errors during summer related to the type of precipitation (solid/liquid, wet/dry snow), C_{prec} was reduced for the summer months to 25 % of its value (Sevruk, 1981). Above a critical elevation Z_{crit}, precipitation is set to no longer increase linearly (Alpert, 1986). Our selected value of Z_{crit} approximated the elevation for which a decrease in accumulation was observed on long-term monitored glaciers situated in the Tien Shan and Caucasus (WGMS, 2013). All parameters used are summarized in Table 3.

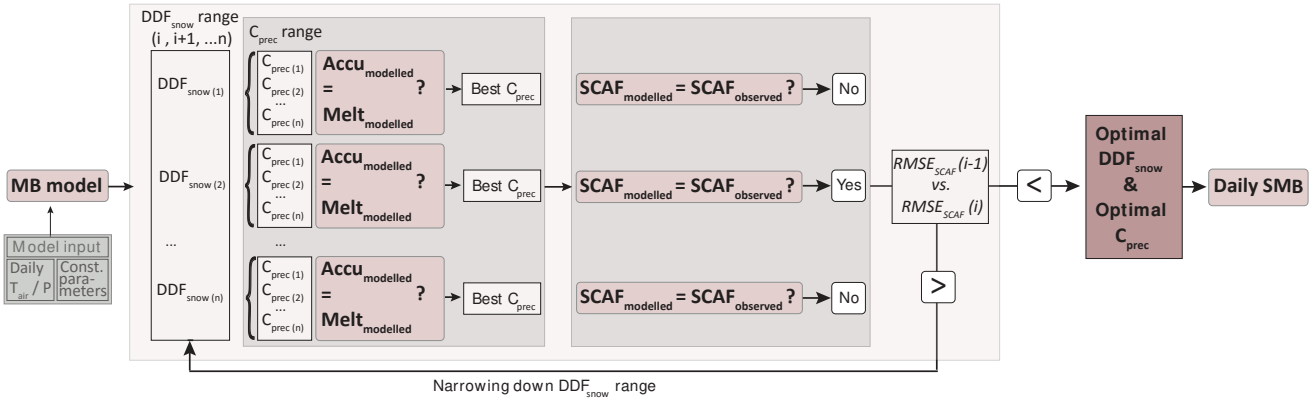

Figure 4. Calibration procedure to obtain an ideal combination of DDF_{snow} and C_{prec}. An initial range for DDF_{snow} and C_{prec} was narrowed down through a comparison with TSL observations until an optimal solution for both parameters was found. First, for each initial value of DDF_{snow}, the best value of C_{prec} was determined, constraining the modelled cumulative melt ($Melt_{modelled}$) at the TSL position to agree with the modelled winter snow accumulation ($Accu_{modelled}$) for the same location. Second, the performance of each DDF_{snow} was evaluated to narrow down the range of DDF_{snow} by comparing the $RMSE_{SCAF}$ of the modelled and observed snow-covered area fractions (SCAF). This was repeated until an optimal solution is reached.

3.6.1 Model calibration

We calibrated C_{prec} and DDF_{snow}, keeping R_{DDF} constant. C_{prec} and DDF_{snow} were calibrated annually and for each glacier separately to correctly represent the winter snow accumulation and the melt rate. To calibrate C_{prec}, we relied on the fact that, at the position of the TSL, ice melt had not yet started but all winter snow was melted. The modelled cumulative melt, calculated at the position of the observed snow line, is thus interpreted as the total amount of accumulated winter snow that melted from the onset of the ablation season until the TSL observation date. Using the melt model, we can infer the winter accumulation at the beginning of the ablation season along each observed TSL. This quantity needs to agree with the directly modelled snow accumulation at the end of the winter season. DDF_{snow} was calibrated to best represent all SCAF observations of one ablation season (Fig. 4).

As C_{prec} and DDF_{snow} depend on each other, overestimation of DDF_{snow} could cause an overestimation of C_{prec}, and vice versa, without affecting the modelled position of the snow line and the SCAF. To overcome this problem, the values of C_{prec} and DDF_{snow} were constrained to remain within realistic bounds. Through an iterative calibration procedure, we aimed at finding the best possible parameter combination without the need of any additional information.

First, we defined a plausible range for DDF_{snow} and C_{prec} for all three glaciers based on the literature (Hock, 2003; Liu and Liu, 2016) (Table 3). For each DDF_{snow}, an optimal parameter C_{prec} was calibrated through iteratively narrowing a plausible range of initial values of C_{prec} (Fig. 4). In this way, the RMSE between the directly modelled winter snow accumulation $Accu_{modelled}$ and the modelled cumulative melt from the onset of the ablation season to each observation date $Melt_{modelled}$ was minimized until no further improvement of the RMSE was observed.

Second, the performance of each DDF_{snow} with its optimal C_{prec} pair, was evaluated based on the $RMSE_{SCAF}$ between the observed $SCAF_{obs}$ and the modelled $SCAF_{modelled}$ for all available snow line observations within 1 year (Fig. 4). The range of DDF_{snow} was narrowed around the best solution and the optimization process was restarted until no further significant improvement of the $RMSE_{SCAF}$ was observed. The calibration procedure was repeated for each year individually.

A minimum of two images was needed to enable application of our calibration approach. The influence of the image frequency and distribution was assessed in detail with sensitivity experiments described in Sect. 4. In a last step, the calibrated model was rerun with the ideal parameter set. This TSL-constrained mass balance model was thus applied to derive continuous daily SMB series that agreed with the snow depletion patterns observed by remote sensing imagery. In the following, we refer to the methodology described above as *snow line approach*.

3.6.2 Adjustments to enable comparison of different methods

Geodetic surveys provide an estimate of the total mass change of a glacier ΔM_{geod}, whereas the results inferred from the snow line approach refer to the surface mass balance B_{sfc} and do not account for internal and basal components of the mass balance (Cogley et al., 2011). For comparing the results, we adjusted the modelled SMB constrained by TSL observations, with an estimate of the internal/basal mass balance of $+0.07\,\mathrm{m\,w.e.\,yr^{-1}}$ for Abramov (Barandun et al., 2015), $+0.08\,\mathrm{m\,w.e.\,yr^{-1}}$ for Golubin (Aizen et al.,

Table 2. Survey period of glaciological measurement for each glacier and each year.

Abramov	Golubin	Glacier no. 354
	10 Sept 2010–17 Aug 2011	5 Sept 2010–12 Aug 2011
26 Aug 2011–22 Aug 2012	17 Aug 2011–29 Aug 2012	12 Aug 2011–14 Aug 2012
22 Aug 2012–15 Aug 2013	29 Aug 2012–25 Aug 2013	14 Aug 2012–23 Jul 2013
15 Aug 2013–18 Aug 2014	25 Aug 2013–17 Aug 2014	23 Jul 2013–3 Sept 2014
18 Aug 2014–27 Aug 2015	27 Aug 2014–9 Aug 2015	3 Sept 2014–14 Aug 2015
27 Aug 2015–1 Aug 2016	9 Aug 2015–14 Sept 2016	14 Aug 2015–29 Aug 2016

1997) and $+0.04\,\mathrm{m\,w.e.\,yr^{-1}}$ for Glacier no. 354 (Kronenberg et al., 2016). Values are positive due to a significant amount of refreezing of meltwater in cold firn.

To compare the results of the different methods, the time periods covered by the data sets also needed to be homogenized. We thus adjusted the observation period of the modelled mass balance constrained by TSL observations to exactly match the respective periods of geodetic and glaciological mass balance. However, the final results $B_{\mathrm{sfc(fix)}}$ derived from the snow line approach are presented for the fixed dates of the hydrological year (1 October to 30 September) and do not include internal/basal mass balance.

4 Uncertainties and model sensitivity

4.1 Glaciological surface mass balance

Uncertainty σ_{glac} related to the direct glaciological measurements for Abramov was adopted from Barandun et al. (2015) and for Glacier no. 354 from Kronenberg et al. (2016). Uncertainties concerning the SMB of Golubin were calculated after Kronenberg et al. (2016). Uncertainties regarding all three glaciers range between 0.24 and $0.30\,\mathrm{m\,w.e.\,yr^{-1}}$ (Table 4). For a sensitivity experiment we artificially shifted temperature and precipitation series used for the model-based extrapolation by $\pm 1\,^{\circ}\mathrm{C}$ and $\pm 25\,\%$. The resulting glacier-wide SMB indicates a very small sensitivity to the meteorological input data with a standard deviation of $< 0.01\,\mathrm{mm\,w.e.\,yr^{-1}}$. We strictly refer to the annual SMB obtained for the measurement dates (Table 2).

4.2 Geodetic mass balance

The total uncertainty of the geodetic mass balance includes a random and systematic error. We followed Brun et al. (2017) to compute the random error of the geodetic mass balance estimate but did not assess the systematic error. Uncertainties in elevation differences were quantified by computing the area-weighted mean of the absolute difference off-glacier in 50 m altitude bins. The resulting values for Abramov, 1.0 m for 2003–2015 and 0.6 m for 2011–2015, and for Glacier no. 354, 0.7 m for 2012–2015, are in line with the uncertainty of 1.3 m found over the Mont Blanc area through a comparison of similar satellite data to elevation differences measured in situ (Berthier et al., 2014). For Golubin, a value of 1.6 m indicates slightly lower DEM quality. The uncertainty related to the density assumption for converting volume to mass change was assumed to be $\pm 60\,\mathrm{kg\,m^{-3}}$ for time intervals larger than 5 years Huss (2013). For shorter periods, we used a more conservative estimate of $\pm 120\,\mathrm{kg\,m^{-3}}$. The elevation uncertainty for unmeasured glacier zones was roughly estimated to be five times as large as the uncertainty determined for measured locations. We assumed independence between the different error components and combined them as the root sum square (RSS) to the total uncertainty for the geodetic mass balance, σ_{geod}.

4.3 Surface mass balance modelling constrained by snow line observations

The uncertainty introduced by the mass balance model constrained by TSL observations σ_{tsl} depends on (1) the delineation accuracy of the SCAF, σ_{map}, (2) the image frequency and distribution throughout the ablation season, σ_{dis}, (3) the DEM quality, σ_{DEM}, (4) the meteorological input data, σ_{meteo}, and (5) the uncertainty in constant model parameters, σ_{para} (Table 4). The individual components were estimated as follows:

1. The accuracy of the mapped SCAF is dependent on the positioning and the transect of the snow line, the georeferencing of the images and the extrapolation of the snow line to invisible areas (Huss et al., 2013). The limit between snow- and ice-covered areas is often not a clear line but rather a transition zone, especially for glaciers with superimposed ice. To account for the total uncertainty related to the mapping procedure, we identified the upper- and lowermost positions of the surface that could be classified as either snow or ice on each available image. Hence this zone included all observed ambiguous areas, such as cloud-covered regions, shading, superimposed ice or invisibility due to reduced image quality (e.g. Landsat 7 SLC-off void-stripes, invisible areas on photographs). We interpreted the zone to be either entirely snow-covered or entirely snow-free. The standard deviation of the minimal, maximal and optimal SCAF was used as an uncertainty. This uncertainty

Table 3. Constant model parameters. The temperature lapse rate for Abramov was adopted from Barandun et al. (2015) and for Golubin and Glacier no. 354 from Aizen et al. (1995). $\delta T/\delta z$, $\delta P/\delta z$, Z_{crit} and R_{DDF} are held constant throughout the entire modelling period. The initial parameter ranges of DDF_{snow} and C_{prec}, as well as the mean value obtained from annual calibration, is given with its standard deviation.

Parameter	Abramov	Golubin	Glacier no. 354	Unit
$\delta T/\delta z$	−4.8	−6.3	−6.7	°C km^{-1}
$\delta P/\delta z$	6.4	4.5	1.5	10^{-4} m^{-1}
R_{DDF}	1.57	1.36	1.06	–
Z_{crit}	4400	4000	4500	m a.s.l
Annually variable model parameters				
Initial range				
DDF_{snow}	3.5–5.5	3.0–5.5	1.5–4.5	mm day^{-1} °C^{-1}
C_{prec}	1.75–3.0	1.5–3.0	1.0–3.5	–
Best combination				
DDF_{snow}	4.54 ± 0.74	5.09 ± 0.46	3.04 ± 0.66	mm day^{-1} °C^{-1}
C_{prec}	2.23 ± 0.40	1.46 ± 0.31	2.35 ± 0.29	–

was calculated for each image individually. To evaluate the corresponding effects on calculated SMB, the model was rerun with the maximal and the minimal possible SCAF. The standard deviation of the SMB, σ_{map}, ranged between 0.06 and 0.09 m w.e. yr^{-1} for the three glaciers.

2. To estimate the effect of varying image availability, we repeated the modelling using different snow line observation frequencies and temporal distributions throughout the summer for calibration. Due to limited image availability, this could only be conducted for the few years in which many images were available (Fig. 3). We used the results to create a look-up table that linked the image frequency, the distribution over the ablation season and the last observation date of the season to an uncertainty estimate in the calculated annual SMB, σ_{dis}. Tests showed that the model reacts more sensitively to image distribution than to reduced image frequency (Fig. 5). A minimum of two images well distributed throughout the ablation season (i.e. at the beginning/middle and at the end) is sufficient to achieve reliable SMB estimates. Greater uncertainties were found if images were concentrated on, for example, a few days at the beginning of the ablation season (Fig. 5). In this case, higher image frequency cannot compensate for the missing information on the snow depletion pattern. An image taken towards the end of the ablation season is more important than images from the beginning of the summer. Our assessment of image availability resulted in smaller uncertainties for Abramov ($\sigma_{dis} = 0.09$ m w.e. yr^{-1}) than for Golubin ($\sigma_{dis} = 0.16$ m w.e. yr^{-1}) and for Glacier no. 354 ($\sigma_{dis} = 0.18$ m w.e. yr^{-1}) (Table 4).

Table 4. Overall average uncertainties related to the three methods used, namely the glaciological σ_{glac}, geodetic σ_{geod} and TSL-constrained modelled mass balances σ_{tsl} for all three investigated glaciers in m w.e. yr^{-1}. Additionally, the uncertainty for each component of the snow line approach is specified. σ_{map} shows the uncertainty of the TSL delineation, σ_{dis} the uncertainty related to image frequency and distribution and σ_{DEM} to the DEM. σ_{meteo} indicates the uncertainty introduced by the meteorological input data and σ_{para} the one by the model parameter choice.

Uncertainty	Abramov	Golubin	Glacier no. 354
Glaciological SMB			
σ_{glac}	0.25	0.30	0.24
Geodetic mass balance			
σ_{geod}	0.16 (2003–2015) 0.26 (2011–2015)	0.37	0.32
SMB from snow line approach			
σ_{tsl}	0.27	0.32	0.36
σ_{map}	0.05	0.06	0.09
σ_{dis}	0.03	0.16	0.18
σ_{DEM}	0.12	0.03	0.02
σ_{meteo}	0.13	0.23	0.14
σ_{para}	0.20	0.17	0.20

3. To estimate the uncertainty caused by the DEM used for the modelling, we compared our results to those obtained from model runs that used lower-resolution DEMs. For this experiment, we replaced the high-resolution DEM with the SRTM (Shuttle Radar Topographic Mission) DEM. This enabled us to both investi-

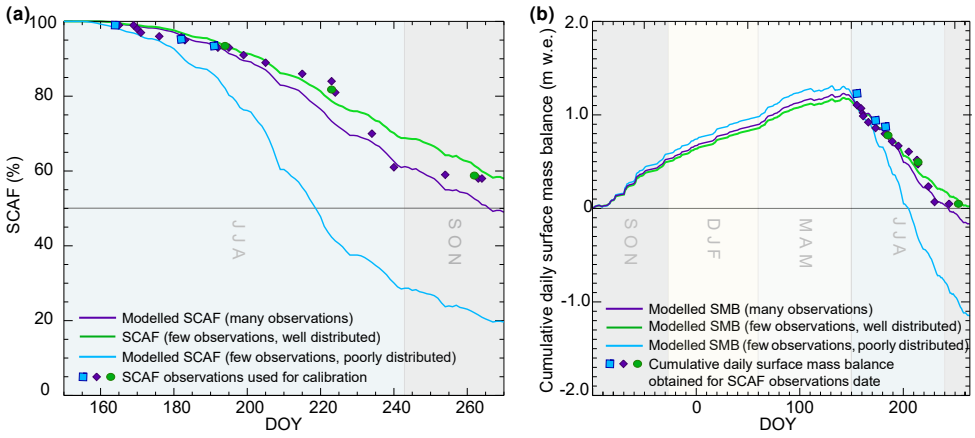

Figure 5. Examples of the **(a)** daily SCAF and **(b)** cumulative daily SMB obtained with different sets of image frequency and distribution for Abramov in 2016. TSL observation dates used to calibrate the model are indicated with symbols. The modelled daily SCAF and cumulative daily SMB and their corresponding TSL observations are shown with the same colour. Three images were used at the beginning of the ablation season (blue), three images were well distributed throughout the ablation season (green) or all available images (purple) were used.

gate the sensitivity of the results to DEM quality and to assess our assumption of unchanged topography during the entire study period. The effects of a reduced DEM quality for all three glaciers were found to be small ($\sigma_{\mathrm{DEM}} < 0.03\,\mathrm{m\,w.e.\,yr^{-1}}$).

4. We investigated the uncertainty related to the meteorological input data, σ_{meteo}, by rerunning the model with a climatological average daily temperature and precipitation series for each glacier instead of the actual meteorological series. The test assessment revealed an RMSE of $0.13\,\mathrm{m\,w.e.\,yr^{-1}}$ for the annual SMB of Abramov, of $0.23\,\mathrm{m\,w.e.\,yr^{-1}}$ for Golubin and $0.14\,\mathrm{m\,w.e.\,yr^{-1}}$ for Glacier no. 354 (Fig. 6). These results demonstrate a relatively low sensitivity of our model approach to daily meteorological input data. With the chosen calibration procedure the model parameters $\mathrm{DDF_{snow}}$ and C_{prec} are adjusted to best represent the TSL observations for each year and glacier individually. The modelled SMB are thus closely tied to the snow line observations and exhibit a reduced dependence from meteorological input data. This underlines the potential of our methodology for regional application based on minimal input data.

5. To test the uncertainty introduced by the constant (i.e. uncalibrated) model parameters, $\delta T/\delta z$, $\delta P/\delta z$ and the R_{DDF} were varied by $\pm 25\,\%$ for each glacier and year. A mean standard deviation, σ_{para}, of around $0.17\,\mathrm{m\,w.e.\,yr^{-1}}$ was found. We additionally tested the behaviour of the model relative to the individual parameters and identified a higher sensitivity to $\delta T/\delta z$ and R_{DDF}, whereas sensitivities to the other parameters were minor (Table 5).

Components 1 to 5 are assumed to be independent of each other and are combined as the RSS to represent the total error of the annual SMB σ_{tsl} obtained from the snow line approach. We then averaged the annual error over the different periods to compute the overall uncertainty.

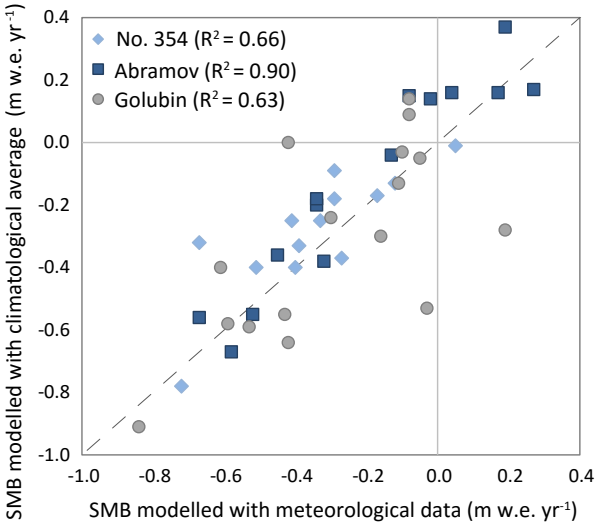

Figure 6. Comparison between the annual SMB obtained from the TSL-constrained model when using meteorological and climatological average daily data for Abramov, Golubin and Glacier no. 354.

Table 5. Model sensitivity to the different constant input parameters for each glacier in $\mathrm{m\,w.e.\,yr^{-1}}$. See text for details on the experiments.

Sensitivity	Abramov	Golubin	Glacier no. 354
$\delta T/\delta z$	0.06	0.14	0.05
$\delta P/\delta z$	0.07	0.08	0.01
R_{DDF}	0.11	0.25	0.06

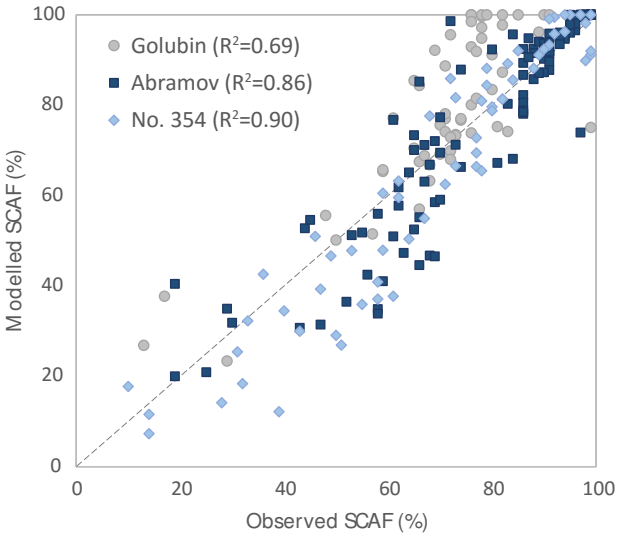

Figure 7. Comparison between observed and modelled SCAF for Abramov, Golubin and Glacier no. 354.

5 Results

5.1 Long-term surface mass balances derived from snow line approach

We found that the mass balance model constrained by TSL observations is capable of representing the observed SCAFs on satellite and terrestrial camera images within ±8 % for Abramov, ±13 % for Golubin and ±9 % for Glacier no. 354 (Fig. 7). Comparing the SCAF observed on camera and on space-borne images for the same day reveals a RMSE of 2.5 %. However, tests showed that the influence of the image source (terrestrial/space-borne) on the inferred SMB is negligible.

Annual glacier-wide modelled surface mass balances constrained by TSL observations, calculated for Abramov (1998–2016), for Golubin (2000–2016) and for Glacier no. 354 (2004–2016), are predominantly negative (Fig. 8 and Table 6). Study periods depend on the data availability for each glacier. Abramov exhibited a mean annual SMB of -0.30 ± 0.19 m w.e. yr^{-1} from 2004 to 2016. For Golubin and Glacier no. 354 slightly more negative annual average balances of -0.41 ± 0.33 and -0.36 ± 0.32 m w.e. yr^{-1} were calculated for the same time period (Table 6). Length change measurements underline the observed negative balance regime of all three glaciers Hoelzle et al. (2017). A significant glacier retreat was observed for the last century. A first speed-up of frontal retreat occurred in the 1980s and acceleration was observed in the last decade. However, no clear acceleration of mass loss for the three glaciers was identified over the investigated periods. Two phases of close-to-zero SMB could be recognized (2002–2005 and 2009–2011) for all glaciers. A lower standard deviation of annual mass balances from 2004 to 2016 is found for Glacier no. 354 (0.19 m w.e. yr^{-1}) than for Golubin (0.4 m w.e. yr^{-1}) and Abramov (0.29 m w.e. yr^{-1}), which indicated higher interannual variability for the latter two. Glacier no. 354, receiving lower amounts of total annual precipitation, showed a smaller mass turnover and had a positive balance only in 2009 (Table 6). For Golubin most negative values were found in 2012 and 2014. Abramov and Golubin also had strongly negative balances in 2006 and 2008. For Abramov, the TSL observations indicated that the snow line rose close to the upper edge of the glacier at the end of August. For Golubin, observations of the last image of the season showed that the SCAF decreased to less than 45 % in mid-August in 2006, similarly to 2001 and 2015. The ablation season typically stretched until the end of September, and summer snowfalls during this month were rare (Aizen et al., 1995), likely leading to continued mass loss. Data availability, however, was rather critical for Golubin in 2008, which is also reflected by the larger uncertainties. The last TSL observation dates from as early as the end of July.

Table 6. Annual, glacier-wide SMB for the three glaciers for the hydrological year $B_{\mathrm{sfc(fix)}}$ in m w.e. yr^{-1} inferred from the mass balance model constrained by TSL observations.

Year	Abramov	Golubin	Glacier no. 354
1998	-0.10 ± 0.21		
1999	$+0.14 \pm 0.19$		
2000	-0.69 ± 0.25	-0.07 ± 0.47	
2001	-0.22 ± 0.21	-0.62 ± 0.20	
2002	$+0.16 \pm 0.16$	-0.13 ± 0.15	
2003	-0.31 ± 0.19	-0.04 ± 0.51	
2004	-0.43 ± 0.22	-0.19 ± 0.35	-0.33 ± 0.28
2005	$+0.03 \pm 0.14$	-0.03 ± 0.24	-0.39 ± 0.24
2006	-0.59 ± 0.32	-0.85 ± 0.35	-0.29 ± 0.21
2007	-0.19 ± 0.18	-0.52 ± 0.24	-0.40 ± 0.26
2008	-0.84 ± 0.28	-1.42 ± 0.52	-0.27 ± 0.47
2009	$+0.07 \pm 0.18$	-0.04 ± 0.43	$+0.05 \pm 0.24$
2010	$+0.25 \pm 0.17$	-0.42 ± 0.30	-0.22 ± 0.23
2011	-0.29 ± 0.16	$+0.26 \pm 0.39$	-0.17 ± 0.39
2012	-0.65 ± 0.20	-0.21 ± 0.23	-0.67 ± 0.42
2013	-0.23 ± 0.16	-0.41 ± 0.36	-0.41 ± 0.43
2014	-0.44 ± 0.17	-0.62 ± 0.31	-0.72 ± 0.55
2015	-0.25 ± 0.16	-0.55 ± 0.24	-0.51 ± 0.31
2016	-0.34 ± 0.17	-0.27 ± 0.31	-0.29 ± 0.10
2004–2016	-0.30 ± 0.19	-0.41 ± 0.33	-0.36 ± 0.32

5.2 Comparison to glaciological and geodetic mass balances

The glaciological and geodetic surveys delivered two extensive and independent data sets for validation of the modelled mass balance series constrained by TSL observations. Joint analysis of the data sets permitted robust conclusions

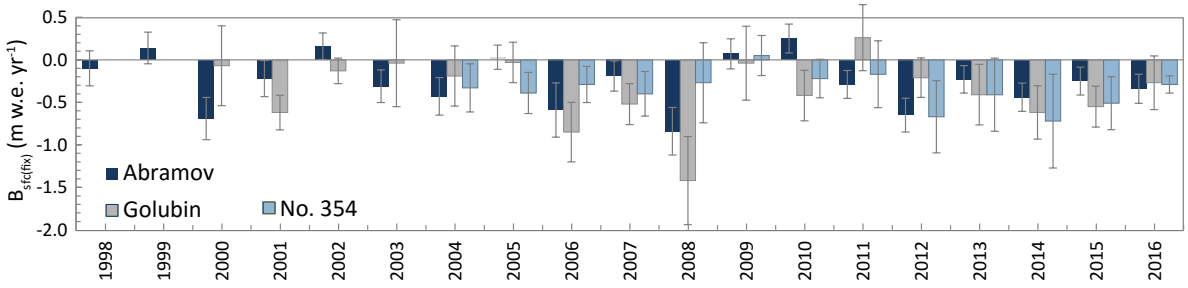

Figure 8. Modelled annual SMB $B_{sfc(fix)}$ constrained by snow line observations for all three glaciers for each hydrological year.

Table 7. Annual SMB $B_{sfc(meas)}$ for the measurement periods (i.e. exact dates of the surveys, Table 2) based on direct glaciological measurements and on the TSL-constrained model for the three glaciers in m w.e yr^{-1}.

	Abramov		Golubin		Glacier no. 354	
Year	Glaciological	TSL-constrained	Glaciological	TSL-constrained	Glaciological	TSL-constrained
2011			-0.06 ± 0.30	-0.05 ± 0.39	-0.21 ± 0.27	$+0.34 \pm 0.39$
2012	-0.29 ± 0.30	-0.47 ± 0.20	-0.14 ± 0.30	$+0.06 \pm 0.23$	-0.52 ± 0.26	-0.74 ± 0.42
2013	-0.31 ± 0.34	-0.27 ± 0.16	-0.10 ± 0.30	-0.07 ± 0.36	-0.54 ± 0.25	-0.45 ± 0.43
2014	-0.74 ± 0.10	-0.50 ± 0.17	-1.56 ± 0.30	-1.44 ± 0.31	-0.68 ± 0.22	-0.74 ± 0.55
2015	-0.24 ± 0.25	-0.65 ± 0.16	-0.62 ± 0.30	-0.45 ± 0.24	-0.68 ± 0.24	-0.60 ± 0.31
2016	$+0.38 \pm 0.25$	$+0.24 \pm 0.17$	$+0.36 \pm 0.30$	-0.04 ± 0.31	-0.41 ± 0.24	-0.26 ± 0.10
2011–2016	-0.24 ± 0.25	-0.33 ± 0.17	-0.35 ± 0.30	-0.33 ± 0.31	-0.51 ± 0.24	-0.41 ± 0.37

to be drawn about the mass change and its temporal dynamics over the past 2 decades. The glaciological SMB measurements showed good agreement with the SMB inferred using TSL observations for the same time periods (Table 7). Exact survey dates are given in Table 2. Annual glaciological SMB was reproduced with an RMSE of less than ± 0.26 m w.e. yr^{-1} for all three glaciers using the TSL approach (Fig. 9). For Golubin and Glacier no. 354, the glaciological SMB was slightly more negative than the modelled SMB (Table 7). For Abramov, on the other hand, the glaciological SMB was somewhat less negative than the TSL-constrained model results. In general, a satisfactory agreement was obtained between the two methods for all three glaciers (Fig. 9). Squared correlation coefficients between TSL-constrained model results and glaciological SMB ranged between $r^2 = 0.63$ (Abramov) and $r^2 = 0.90$ (Golubin).

Table 8 and Fig. 10 summarize the results obtained from the different geodetic surveys. For the comparison with the geodetic mass change, an estimate for internal/basal mass balance was added to the modelled SMB constrained by TSL observations (see Sect. 3.6.2) and referred to as the modelled total mass change constrained by TSL observations. The geodetic method reveals a total mass balance of -0.30 ± 0.37 m w.e. yr^{-1} for Golubin from 8 September 2006 to 1 November 2014 (Fig. 10). The corresponding total modelled mass balance constrained by TSL observations

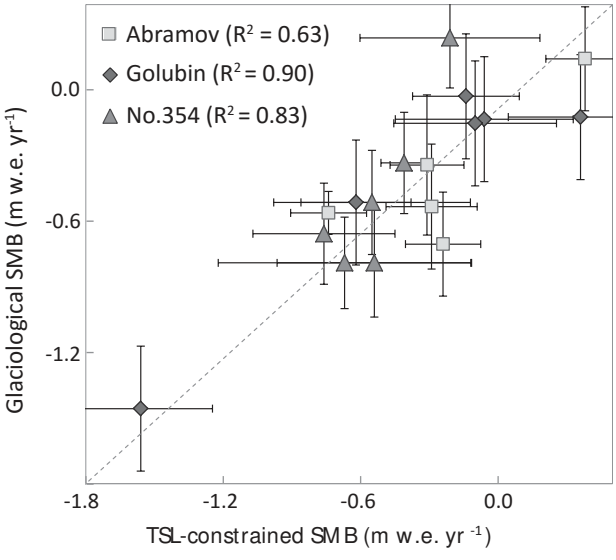

Figure 9. Comparison of modelled annual SMB constrained by TSL observations and glaciological SMB for Abramov, Golubin and Glacier no. 354. Uncertainties in the annual SMB are indicated.

was slightly more negative with -0.38 ± 0.35 m w.e. yr^{-1} for the same period (Table 8 and Fig. 11). Comparison of digital elevation models indicated that Glacier no. 354 had a mass balance of -0.58 ± 0.31 m w.e. yr^{-1} from 27 July 2012

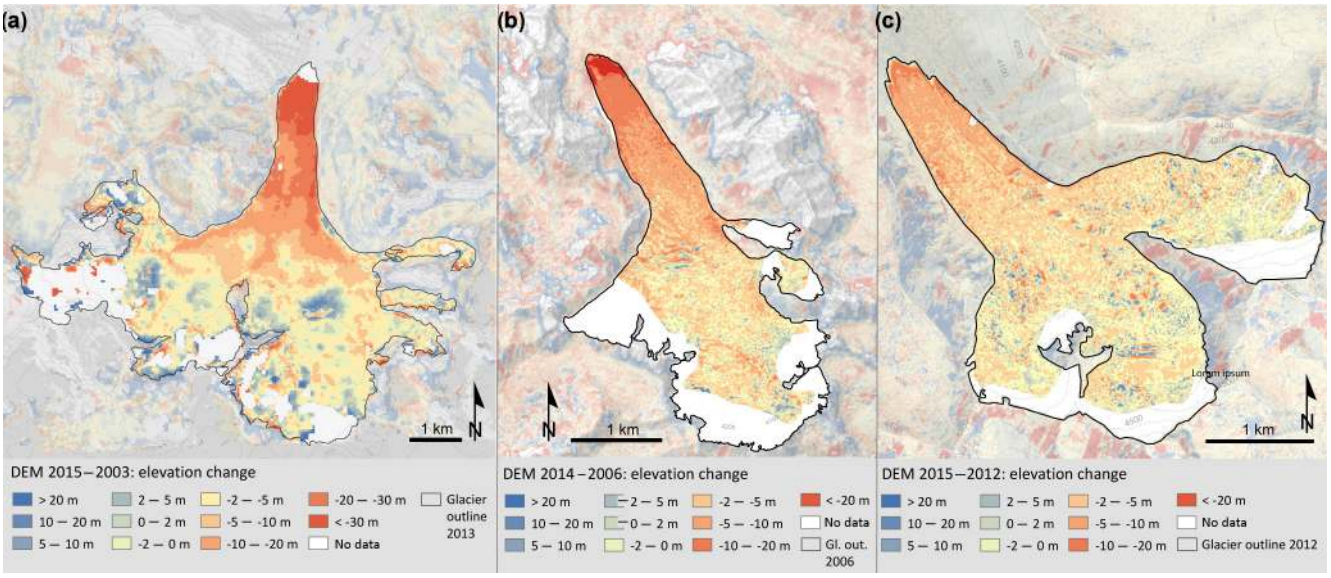

Figure 10. Geodetic mass balance for **(a)** Abramov from 2003 to 2015, **(b)** Golubin from 2006 to 2014 and for **(c)** Glacier no. 354 from 2012 to 2015.

to 1 October 2015 (Fig. 10) and -0.42 ± 0.07 m w.e. yr^{-1} from 1 September 2003 to 27 July 2012 (Kronenberg et al., 2016). The total annual mass changes for the same time intervals derived from the TSL approach were -0.53 ± 0.43 and -0.25 ± 0.31 m w.e. yr^{-1}. For the first period, the results are in good agreement, whereas for the second period the mass balance model constrained by snow line observations indicates a significantly less negative mass balance (Fig. 11). For Abramov, geodetic mass balance values of -0.39 ± 0.16 m w.e. yr^{-1} from 27 August 2003 to 1 September 2015 and -0.36 ± 0.26 m w.e. yr^{-1} from 29 November 2011 to 1 September 2015 were calculated. For the same periods, the snow line model reveals total mass changes of -0.25 ± 0.20 m w.e. yr^{-1} and -0.43 ± 0.17 m w.e. yr^{-1}. For the first period, the modelled mass balance constrained by snow line observations indicates a less negative mass balance, whereas the second period is in good agreement (Table 8 and Fig. 11). For all three glaciers and periods studied the differences are within the error margins.

Table 8. Geodetic mass change $\Delta M_{\text{geod(meas)}}$ and the total annual mass change derived from the snow line approach $\Delta M_{\text{tsl(meas)}}$ for the three glaciers and for the periods corresponding to the geodetic surveys in m w.e. yr^{-1}.

	$\Delta M_{\text{geod(meas)}}$	$\Delta M_{\text{tsl(meas)}}$
Abramov		
2003–2015	-0.39 ± 0.16	-0.25 ± 0.20
2011–2015	-0.36 ± 0.26	-0.43 ± 0.17
Golubin		
2006–2014	-0.30 ± 0.37	-0.38 ± 0.35
Glacier no. 354		
2003–2012	-0.42 ± 0.07	-0.25 ± 0.31
2012–2015	-0.58 ± 0.31	-0.53 ± 0.43

6 Discussion

6.1 More accurate modelling through integrating TSL observations

In order to demonstrate the advantage of using TSL observations on repeated remote sensing data throughout the melt season to increase the confidence in mass balance modelling, we ran the same accumulation and temperature-index model without the use of snow lines or any other direct observations to calibrate for all three glaciers from 2004 to 2016 (see Sect. 3.6). The same constant parameters were used (Table 3). We chose C_{prec} to account for a 20 % measurement error of observed precipitation (Sevruk, 1981) and a combination for DDF_{ice} (7.0 mm day^{-1} °C^{-1}) and DDF_{snow} (5.5 mm day^{-1} °C^{-1}) as recommended by Hock (2003) for the former Soviet territory, for all three glaciers. Similar values were used to model glaciers in the Tien Shan and Himalayas (e.g. Zhang et al., 2006; Wu et al., 2011; Shea et al., 2015). All parameters were held constant over time. Figure 12 shows the difference between the cumulative SMB derived from our model constrained by TSL observations and the results obtained with an unconstrained mass balance model. The results clearly indicate the potential of the snow line approach to infer SMB series of unmeasured glaciers without any additional information. The unconstrained mass

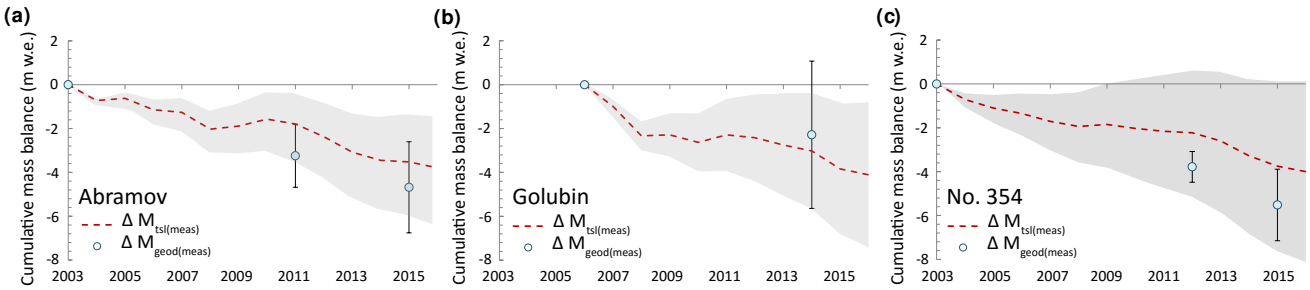

Figure 11. Cumulative TSL-constrained modelled mass change $\Delta M_{\mathrm{tsl(meas)}}$ (red) in comparison to the geodetic mass change $\Delta M_{\mathrm{geod(meas)}}$ (circles) for **(a)** Abramov, **(b)** Golubin and **(c)** Glacier no. 354. The shading indicates the uncertainty range of the mass change from the snow line approach.

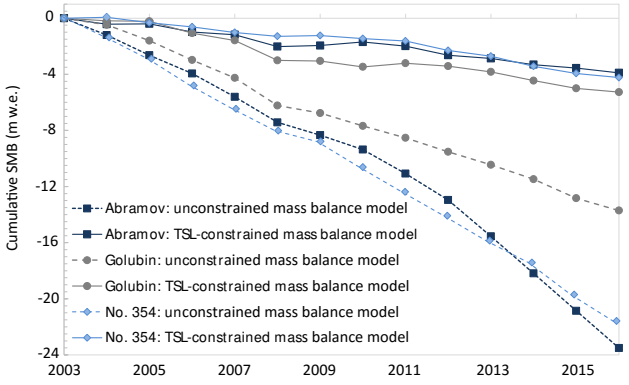

Figure 12. Comparison of the cumulative SMB derived from unconstrained mass balance modelling to the results obtained from TSL-constrained modelling from 2004 to 2016.

balance model overestimates mass loss by almost five times for Abramov and for Glacier no. 354, whereas mass loss for Golubin is about three times higher (Fig. 12).

6.2 Intercomparison of methods to determine glacier mass balance

A satisfying agreement was found between all three independent methods used to compute glacier-wide mass balance for the three benchmark glaciers in the central Tien Shan and Pamir-Alay for the past 2 decades. In the following, we discuss the shortcomings and advantages of each method and point out the limitations of the individual approaches.

The snow line model reproduces the direct measurements well and shows a satisfactory performance for all three glaciers (Tables 8, 6 and Fig. 13). For Glacier no. 354, a larger misfit between the glaciological SMB and the TSL-constrained model results was found, especially for 2011. A possible reason might be the limited stake network at the initiation of the monitoring programme, errors of the stake readings and an unknown measurement date for some ablation stakes, affecting the calculation of the glaciological SMB for the considered year. Discrepancies between the two approaches are also found for Golubin for 2016 and for Abramov for 2015. For Abramov, summer snowfalls in mid-August 2015 stopped the ablation season early. This pattern is mirrored in the daily SMB derived from the snow line approach. For Golubin, the last snow line observation is from the end of August and matches the field observations. No clear indication of a poor performance of the snow line approach could thus be identified for both glaciers for the considered years.

A significant problem is related to the varying measurement periods of the glaciological SMBs for the selected glaciers (Table 2). Due to changing period lengths, the data do not always represent a complete mass balance year and might thus not be representative, making comparisons of the results with other methods, glaciers and regions difficult. Interpretation of the results, their contextualization and application in other study fields, such as in hydrology or climatology, are also hampered through the varying and irregular investigation periods. Based on our methodology, we are now able to derive homogenous SMBs for comparable periods of the hydrological year.

An important factor limiting the applicability of mass balance modelling constrained by TSL observations is the dependence on good satellite imagery to map the snow line throughout the ablation season. However, the sensitivity analysis (Sect. 4) shows that a minimum of only two images that are well distributed throughout the ablation season are sufficient to retrieve reliable results. Image availability is most important close to the end of the ablation season. Taking into account the increasing number of satellite sensors that provide a range of possibilities to observe snow lines in the future will partly resolve this limitation. By comparing the TSL-derived daily SMBs for the years in which seasonal in situ measurements are available, we were able to investigate the effect on the results of the two parameters used for model calibration. The mass balance of Golubin is slightly underestimated at the beginning of the ablation season, and hence the modelled melt is also too low (Fig. 13b). This shortcoming of the calibration procedure cannot be overcome without

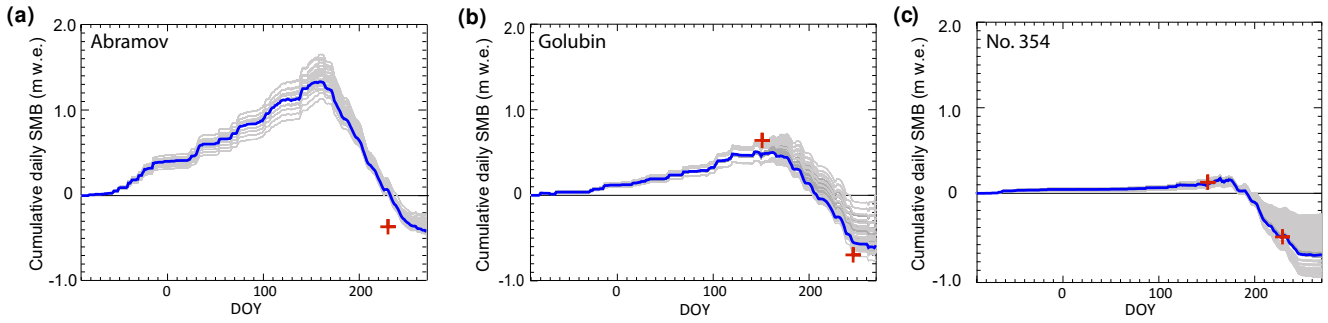

Figure 13. Cumulative daily glacier-wide SMBs inferred from the snow line approach for **(a)** Abramov, **(b)** Golubin and **(c)** Glacier no. 354 for the year 2014 (blue line). The grey lines indicate the spread obtained by using different constant parameters to run the model (Sect. 4) and the red cross indicates the measured glaciological SMB for both the winter and the annual period.

including additional data, such as measurements of winter snow accumulation, which are difficult to obtain from remote glaciers.

SMBs inferred from the snow line approach are closely tied to the representativeness of TSL observations. The method might be able to yield reliable SMB estimates for many glaciers in different climatic regimes in which the TSL is an indicator of the surface mass balance. The relationship between the snow line and the SMB can, however, be challenged when the position of the TSL is blurred by fresh snow or superimposed ice. The applicability of the snow line approach presented here can thus be critical when the TSL on remote sensing data cannot unambiguously be identified. This is mainly a problem for glaciers with a summer accumulation regime due to frequent fresh snowfall and glaciers with a high relevance of superimposed ice.

The geodetic mass balance and the results obtained from the snow line approach agree well, in particular for recent years (Fig. 11). Overall, a slightly greater mass loss is calculated for Abramov and Glacier no. 354 using DEM differencing. Especially during the earlier part of our study period, the mass balance inferred with the snow line approach seems to be not negative enough. Limitations related to the geodetic approach are mainly connected to the limited stereo acquisitions in the first years of the 21st century. In recent years, image availability has strongly increased, but it is still not common to find a suitable scene from the end of the hydrological year for any glacier or region with sufficient quality for a sound geodetic evaluation. Fresh snow or low image contrast (in particular in the accumulation areas) interfere with DEM quality but cannot be avoided and have thus to be corrected for, increasing the uncertainty of the result. We present geodetic mass balances for periods shorter than 5 years, a critical time interval for an accurate volume-to-mass conversion. Huss (2013) showed high variability in the volume-to-mass conversion factor for short observation periods (≤ 3 years), especially for glaciers with close-to-zero mass balances in combination with strongly varying mass balance gradients. For the observation periods considered in this study, annual mass balances were predominantly negative but moderate variations of the mass balance gradients have been observed (Barandun et al., 2015; Kronenberg et al., 2016). We identified a rather large elevation change for the short observation periods and are thus confident that the chosen conversion factor lies within the uncertainty range assigned here (see Sect. 4).

The glaciological and the modelled results constrained by TSL observations refer to SMB components only. The geodetic mass balance, on the other hand, takes into account the total glacier mass change, thus including internal and basal ablation and accumulation. This is a limiting factor for direct comparison. Evidence of refreezing meltwater in cold firn is reported for all three glaciers (Suslov et al., 1980; Aizen et al., 1997; Dyurgerov and Mikhalenko, 1995) and can have a significant effect on the total mass change. The values used in this study to account for internal and basal mass balance are first-order approximations which improve the comparability between the different methods. However, the uncertainties in these estimates are considerable.

6.3 Comparison with other studies

We performed a comprehensive comparison of long-term averages of mass balance derived from the snow line approach to independent studies based on geodetic surveys using different sensors and modelling, both for the investigated glaciers as well as for the regional mass budget (Fig. 14). Note that the study periods vary between the different studies and results might thus not be directly comparable.

For Abramov, we find mass balances in between the results derived by Gardelle et al. (2013) and Brun et al. (2017) based on the comparison of DEMs, overlapping within the respective uncertainty ranges. Mass changes reported by Gardelle et al. (2013) are most likely too positive as SRTM C-Band penetration depth into snow (Kääb et al., 2015; Berthier et al., 2016) might have been underestimated for the cold and dry snow in accumulation areas (Dehecq et al., 2016). The average mass balance for Abramov of -0.38 ± 0.10 m w.e. yr^{-1}

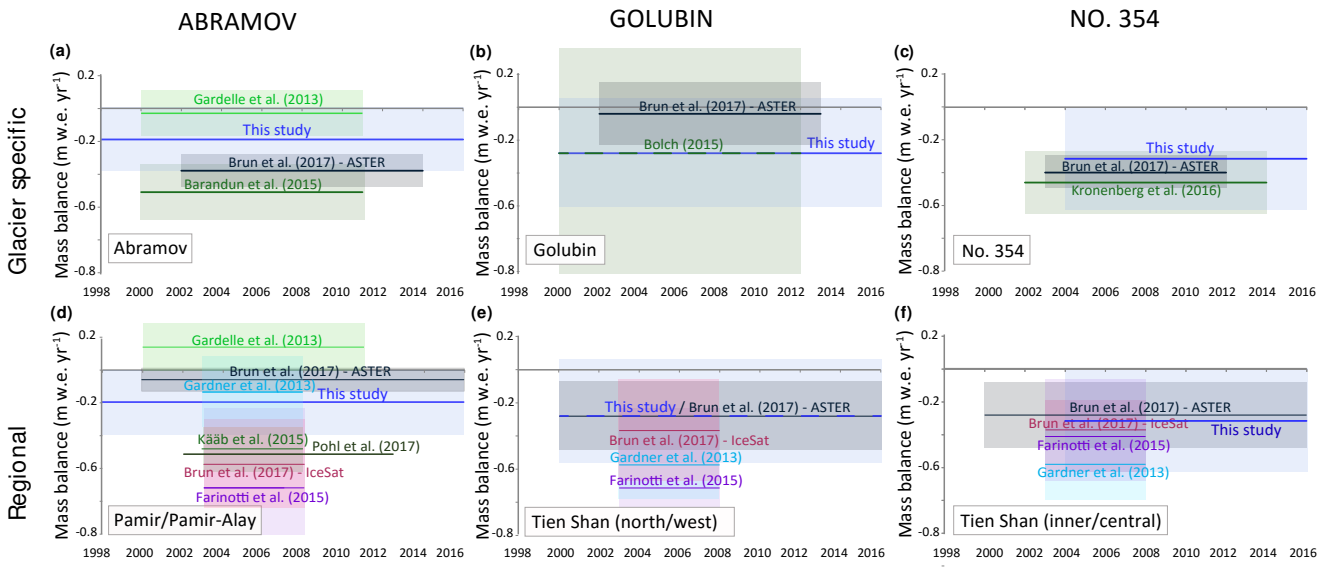

Figure 14. Long-term average mass balances from various studies in comparison with the TSL-constrained modelled mass balance for **(a)** Abramov, **(b)** Golubin and **(c)** Glacier no. 354. Results from the snow line approach for the three glaciers are compared to region-wide mass balance estimates for **(d)** the Pamir, for **(e)** Tien Shan (north/west) and for **(f)** the Tien Shan (central). Lines indicate the mean annual mass balance over the respective periods for each study, and shaded squares represent the corresponding uncertainty. For the study by Brun et al. (2017) results based on ASTER DEMs and IceSat are presented separately.

(2002–2014) derived by Brun et al. (2017) using multi-temporal optical ASTER DEMs indicates a stronger mass loss than the results obtained with the snow line approach. We note, however, that the start and end dates of their geodetic mass balance assessment represent a mean over a mosaic of different dates, thus hampering direct comparison. In addition, the differences are still within their error bounds. The results by Brun et al. (2017) are in line with the geodetic mass balance calculated in the present study for the period 2003 to 2015 based on high-resolution satellite images.

For Golubin, the inferred mass balance is in close agreement with the geodetic mass change reported by Bolch (2015) (Fig. 14b). Brun et al. (2017) computed a mass balance of -0.04 ± 0.19 m w.e. yr^{-1} for $\approx$2002–2013, which is consistently less negative than our estimate but still lies within the respective error bounds. For Glacier no. 354, an excellent agreement between all available mass balance assessments was found (Fig. 14c). Brun et al. (2017) reported a mass balance of -0.46 ± 0.19 m w.e. yr^{-1} for $\approx$2002–2014.

We also compared our results for the investigated glaciers to region-wide assessments in order to investigate their regional representativeness (Fig. 14d–f). Brun et al. (2017) divided the Pamir-Alay and the Pamir into two different regions, whereas Gardner et al. (2013), Gardelle et al. (2013), Kääb et al. (2015) and Farinotti et al. (2015) did not make this distinction. For the Pamir, widely varying mass balance estimates were presented by the different studies, which might be related to the important methodological differences and inconsistent time periods considered. Our results for Abramov are close to the average of the regional studies (Fig. 14d). The interannual variability, and in particular a very negative mass balance in 2008 and positive balance in 2010 for Abramov found in the present study, agrees well with modelled mass balance series reported by Pohl et al. (2017) for the Pamir from 2002 to 2013. The TSL-constrained modelled mass balance for Golubin agrees with the region-wide estimates by Brun et al. (2017) but indicates smaller mass losses than other large-scale studies (Fig. 14e). Close agreement between the different regional studies is found for the central Tien Shan, where Glacier no. 354 is located (Fig. 14f).

7 Conclusions

In this study we used three independent methods to reconstruct robust mass balance series at high temporal resolution for Abramov, Golubin and Glacier no. 354 located in the Pamir-Alay and Tien Shan mountains over the past 2 decades – a period for which very little is known about glacier behaviour. We proposed a methodology to derive glacier SMB series for unmeasured glaciers based on mass balance modelling constrained by repeated TSL observations, relying either on in situ temperature and precipitation data or climate reanalysis data sets. We recommend including TSL observations in the glacier monitoring strategy to reduce uncertainty and to increase the robustness of the data. We used extensive geodetic and glaciological surveys to validate the results and found satisfying agreement between the independent meth-

ods. Our snow line approach reproduced observed annual to decadal SMB for all three glaciers and enabled the calculation of daily SMBs for arbitrary periods and is hence capable of covering the entire hydrological year based on minimal data input. Some of the shortcomings of the glaciological and geodetic surveys could thus be overcome.

The results of all three methods confirm a continuous mass loss of the three glaciers Abramov, Golubin and Glacier no. 354 since ≈ 2000, but no clear SMB trend could be identified for the time period considered. Our results suggest a slightly less negative SMB for Abramov of -0.30 ± 0.19 m w.e. yr^{-1} located in the Pamir-Alay than for the Tien Shan glaciers Golubin of -0.41 ± 0.33 m w.e. yr^{-1} and Glacier no. 354 of -0.36 ± 0.32 m w.e. yr^{-1} from 2004 to 2016. Periods of almost balanced mass budgets were observed from 2002 to 2005 and from 2009 to 2011. The mass balance of 2006 to 2008 was very negative for Abramov and Golubin. Glacier no. 354 showed weaker interannual variability than the other two glaciers. Model sensitivity experiments revealed a relatively small sensitivity to the input parameters and the meteorological data used, indicating a considerable advantage in comparison to conventional mass balance modelling that does not include direct glacier-specific observations. Our results show that, with a minimum of two TSL observations, ideally at the beginning and the end of the ablation season, reliable estimates of the annual SMB can be inferred.

At present, mass balance observations in the Pamir and Tien Shan are relatively sparse but crucially needed to improve our understanding of glacier behaviour in the region and its effect on future water availability. Direct measurements are important but costly and laborious and require an immense logistic effort. For remote and unmonitored regions and countries, lacking in financial resources and infrastructure necessary to support such monitoring programmes, our proposed approach delivers a tool for investigating and reconstructing the SMBs of unmeasured and remote glaciers with minimal effort. The integration of TSL observations into conventional modelling is shown to be highly beneficial for filling the gaps in long-term SMB series for periods for which direct glaciological measurements were discontinued or are missing completely.

Data availability. Measurements and detailed model results are available in the Supplement. Model code and raw data are available upon request from the first author (Martina Barandun) or can be downloaded through official, open-access databases and online portals (see the Supplement for more information).

The Supplement related to this article is available online at https://doi.org/10.5194/tc-12-1899-2018-supplement.

Competing interests. The authors declare that they have no conflict of interest.

Acknowledgements. This study is supported by the Swiss National Science Foundation (SNSF), grant 200021_155903. Additional support by the German Federal Foreign Office in the frame of the CAWa project (http://www.cawa-project.net) and the support of the Federal Office of Meteorology and Climatology MeteoSwiss through the project Capacity Building and Twinning for Climate Observing Systems (CATCOS) Phase 1 & 2, contract nos. 7F-08114.1, 7F-08114.02.01, between the Swiss Agency for Development and Cooperation (SDC) and MeteoSwiss as well as the project CICADA (Cryospheric Climate Services for improved Adaptation), and contract no. 81049674 between the Swiss Agency for Development and Cooperation and the University of Fribourg is equally acknowledged. Etienne Berthier acknowledges support from the French Space Agency (CNES) and the Programme National de Télédétection Spatiale grant PNTS-2016-01. Andreas Kääb and Tobias Bolch acknowledges funding by the ESA (Glaciers_cci project 4000109873/14/I-NB), and the European Union Seventh Framework Program (FP7) under the European Research Council (ERC) contract 320816. We thank Fanny Brun for providing the elevation change data of Abramov, Golubin and Glacier no. 354. Javier Corripio is acknowledged for the software to georeference oblique photographs. We extend our thanks to Tomas Saks, Alyssa Ghirlanda, Abror Gafurov, Marlene Kronenberg, David Sciboz and all others who contributed with fieldwork. We are also grateful for the collaboration of the Central Asian Institute for Applied Geosciences, especially to Bolot Moldobekov for his continuous support. The Kumtor Gold Company provided the meteorological data. We thank Susan Braun-Clarke for the proofreading and linguistic revision. Constructive comments by the anonymous reviewer and Mauri Pelto were very helpful in finalizing the manuscript.

Edited by: Valentina Radic
Reviewed by: Mauri Pelto and one anonymous referee

References

Aizen, V.: Reconstruktiya balansa massy lednika Golubina [Golubin glacier mass balance reconstruction], Mater. Glyatsiol. Issled, 62, 119–126, 1988.

Aizen, V. B., Aizen, E. M., and Melack, J. M.: Climate, snow cover, glaciers, and runoff in the Tien Shan, central Asia, JAWRA Journal of the American Water Resources Association, 31, 1113–1129, 1995.

Aizen, V. B., Aizen, E. M., Melack, J. M., and Dozier, J.: Climatic and hydrologic changes in the Tien Shan, central Asia, J. Climate, 10, 1393–1404, https://doi.org/10.1175/1520-0442(1997)010<1393:CAHCIT>2.0.CO;2, 1997.

Aizen, V. B., Kuzmichenok, V. A., Surazakov, A. B., and Aizen, E. M.: Glacier changes in the Tien Shan as determined from topographic and remotely sensed data, Global Planet. Change, 56, 328–340, 2007.

Alpert, P.: Mesoscale indexing of the distribution of orographic precipitation over high mountains, J. Clim. Appl. Meteorol., 25, 532–545, 1986.

Barandun, M., Huss, M., Sold, L., Farinotti, D., Azisov, E., Salzmann, N., Usubaliev, R., Merkushkin, A., and Hoelzle, M.: Re-analysis of seasonal mass balance at Abramov glacier 1968–2014, J. Glaciol., 61, 1103–1117, https://doi.org/10.3189/2015JoG14J239, 2015.

Berthier, E., Vincent, C., Magnússon, E., Gunnlaugsson, Á. Þ., Pitte, P., Le Meur, E., Masiokas, M., Ruiz, L., Pálsson, F., Belart, J. M. C., and Wagnon, P.: Glacier topography and elevation changes derived from Pléiades sub-meter stereo images, The Cryosphere, 8, 2275–2291, https://doi.org/10.5194/tc-8-2275-2014, 2014.

Berthier, E., Cabot, V., Vincent, C., and Six, D.: Decadal Region-Wide and Glacier-Wide Mass Balances Derived from Multi-Temporal ASTER Satellite Digital Elevation Models. Validation over the Mont-Blanc Area, Front. Earth Sci., 4, 63 pp., 2016.

Bolch, T.: Glacier area and mass changes since 1964 in the Ala Archa Valley, Kyrgyz Ala-Too, northern Tien Shan, Ice and Snow, 55, 28–39, 2015.

Braithwaite, R. J.: Short Notes: Can the Mass Balance of a Glacier be Estimated from its Equilibrium-Line Altitude?, J. Glaciol., 30, 364–368, 1984.

Braithwaite, R. J.: Positive degree-day factors for ablation on the Greenland ice sheet studied by energy-balance modelling, J. Glaciol., 41, 153–160, 1995.

Brun, F., Berthier, E., Wagnon, P., Kääb, A., and Treichler, D.: A spatially resolved estimate of High Mountain Asia glacier mass balances, 2000–2016, Nat. Geosci., 10, 668–673, https://doi.org/10.1038/ngeo2999, 2017.

Chen, Y., Li, W., Deng, H., Fang, G., and Li, Z.: Changes in Central Asia's Water Tower: Past, Present and Future, Scientific Reports, 6, 35458, https://doi.org/10.1038/srep35458, 2016.

Chinn, T.: Glacier fluctuations in the Southern Alps of New Zealand determined from snowline elevations, Arctic Alpine Res., 27, 187–198, https://doi.org/10.2307/1551901, 1995.

Chinn, T.: New Zealand glacier response to climate change of the past 2 decades, Global Planet. Change, 22, 155–168, 1999.

Cogley, J., Hock, R., Rasmussen, L., Arendt, A., Bauder, A., Braithwaite, R., Jansson, P., Kaser, G., Möller, M., Nicholson, L., and Zemp, M.: Glossary of glacier mass balance and related terms, IHP-VII technical documents in hydrology No. 86, IACS Contribution No. 2, https://doi.org/10.5167/uzh-53475, 2011.

Corripio, J.: Snow surface albedo estimation using terrestrial photography, Int. J. Remote Sens., 25, 5705–5729, https://doi.org/10.1080/01431160410001709002, 2004.

Dee, D., Uppala, S., Simmons, A., Berrisford, P., Poli, P., Kobayashi, S., Andrae, U., Balmaseda, M., Balsamo, G., Bauer, P., Bechtold, P., Beljaars, A. C. M., van de Berg, L., Bidlot, J., Bormann, N., Delsol, C., Dragani, R., Fuentes, M., Geer, A. J., Haimberger, L., Healy, S., Hersbach, H., Hólm, E., Isaksen, L., Kållberg, P., Köhler, M., Matricardi, M., McNally, P., Monge-Sanz, B., Morcrette, J., Park, B., Peubey, C., de Rosnay, P., Tavolato, C., Thépaut, J., and Vitart, F.: The ERA-Interim reanalysis: configuration and performance of the data assimilation system, Q. J. Roy. Meteor. Soc., 137, 553–597, https://doi.org/10.1002/qj.828, 2011.

Dehecq, A., Millan, R., Berthier, E., Gourmelen, N., Trouvé, E., and Vionnet, V.: Elevation changes inferred from TanDEM-X data over the Mont-Blanc area: Impact of the X-band interferometric bias, IEEE J. Sel. Top. Appl., 9, 3870–3882, https://doi.org/10.1109/JSTARS.2016.2581482, 2016.

Duethmann, D., Peters, J., Blume, T., Vorogushyn, S., and Güntner, A.: The value of satellite-derived snow cover images for calibrating a hydrological model in snow-dominated catchments in Central Asia, Water Resour. Res., 50, 2002–2021, https://doi.org/10.1002/2013WR014382, 2014.

Dyurgerov, M.: Substitution of long-term mass balance data by measurements of one summer, Zeitschrift für Gletscherkunde und Glazialgeologie, 32, 177–184, 1996.

Dyurgerov, M. and Mikhalenko, V.: Oledeneniye Tien Shanya [Glaciation of Tien Shan], VINITI, Moscow [in Russian], 1995.

Dyurgerov, M., Mikhalenko, V., Kunakhovitch, M., Ushnurtsev, S., Liu, C., and Xie, Z.: On the cause of glacier mass balance variations in the Tian Shan mountains, GeoJournal, 33, 311–317, https://doi.org/10.1007/BF00812879, 1994.

Farinotti, D., Longuevergne, L., Moholdt, G., Duethmann, D., Mölg, T., Bolch, T., Vorogushyn, S., and Güntner, A.: Substantial glacier mass loss in the Tien Shan over the past 50 years, Nat. Geosci., 8, 716–722, https://doi.org/10.1038/ngeo2513, 2015.

Fujita, K., Takeuchi, N., Nikitin, S. A., Surazakov, A. B., Okamoto, S., Aizen, V. B., and Kubota, J.: Favorable climatic regime for maintaining the present-day geometry of the Gregoriev Glacier, Inner Tien Shan, The Cryosphere, 5, 539–549, https://doi.org/10.5194/tc-5-539-2011, 2011.

Gao, X., Ye, B., Zhang, S., Qiao, C., and Zhang, X.: Glacier runoff variation and its influence on river runoff during 1961–2006 in the Tarim River Basin, China, Science China Earth Sciences, 53, 880–891, https://doi.org/10.1007/s11430-010-0073-4, 2010.

Gardelle, J., Berthier, E., Arnaud, Y., and Kääb, A.: Region-wide glacier mass balances over the Pamir-Karakoram-Himalaya during 1999–2011, The Cryosphere, 7, 1263–1286, https://doi.org/10.5194/tc-7-1263-2013, 2013.

Gardner, A., Moholdt, G., Cogley, J., Wouters, B., Arendt, A., Wahr, J., Berthier, E., Hock, R., Pfeffer, W., Kaser, G., Ligtenberg, S., Bolch, T., Sharp, M., Hagen, J., van den Broeke, M., and Paul, F.: A Reconciled Estimate of Glacier Contributions to Sea Level Rise: 2003 to 2009, Science, 340, 852–857, https://doi.org/10.1126/science.1234532, 2013.

GCOS: The Global Observing System for Climate: Implementation Needs, GCOS-200, 325 pp., 2016.

Glazirin, G., Kamnyanskii, G., and Perziger, F.: Regime of the Abramov glacier, Hydrometeo Publishing, Leningrad, 1993.

Goerlich, F., Bolch, T., Mukherjee, K., and Pieczonka, T.: Glacier Mass Loss during the 1960s and 1970s in the Ak-Shirak Range (Kyrgyzstan) from Multiple Stereoscopic Corona and Hexagon Imagery, Remote Sens., 9, 275, https://doi.org/10.3390/rs9030275, 2017.

Hock, R.: A distributed temperature-index ice-and snowmelt model including potential direct solar radiation, J. Glaciol., 45, 101–111, https://doi.org/10.1017/S0022143000003087, 1999.

Hock, R.: Temperature index melt modelling in mountain areas, J. Hydrology, 282, 104–115, 2003.

Hock, R., Kootstra, D.-S., and Reijmer, C.: Deriving glacier mass balance from accumulation area ratio on Storglaciären, Sweden, IAHS-AISH publication, 163–170, 2007.

Hoelzle, M., Azisov, E., Barandun, M., Huss, M., Farinotti, D., Gafurov, A., Hagg, W., Kenzhebaev, R., Kronenberg, M., Machguth, H., Merkushkin, A., Moldobekov, B., Petrov, M., Saks, T., Salzmann, N., Schöne, T., Tarasov, Y., Usubaliev, R., Vorogushyn, S., Yakovlev, A., and Zemp, M.: Re-establishing glacier monitoring in Kyrgyzstan and Uzbekistan, Central Asia, Geosci. Instrum. Method. Data Syst., 6, 397–418, https://doi.org/10.5194/gi-6-397-2017, 2017.

Hulth, J., Rolstad Denby, C., and Hock, R.: Estimating glacier snow accumulation from backward calculation of melt and snowline tracking, Ann. Glaciol., 64, 1–7, https://doi.org/10.3189/2013AoG62A083, 2013.

Huss, M.: Density assumptions for converting geodetic glacier volume change to mass change, The Cryosphere, 7, 877–887, https://doi.org/10.5194/tc-7-877-2013, 2013.

Huss, M. and Hock, R.: Global-scale hydrological response to future glacier mass loss, Nat. Clim. Change, 8, 135–140, https://doi.org/10.1038/s41558-017-0049-x, 2018.

Huss, M., Bauder, A., Funk, M., and Hock, R.: Determination of the seasonal mass balance of four Alpine glaciers since 1865, J. Geophys. Res., 113, F01015, https://doi.org/10.1029/2007JF000803, 2008.

Huss, M., Bauder, A., and Funk, M.: Homogenization of long-term mass balance time series, Ann. Glaciol., 50, 198–206, https://doi.org/10.3189/172756409787769627, 2009.

Huss, M., Sold, L., Hoelzle, M., Stokvis, M., Salzmann, N., Farinotti, D., and Zemp, M.: Towards remote monitoring of sub-seasonal glacier mass balance, Ann. Glaciol., 53, 278–286, https://doi.org/10.3189/2012JoG11J216, 2013.

Kääb, A., Treichler, D., Nuth, C., and Berthier, E.: Brief Communication: Contending estimates of 2003–2008 glacier mass balance over the Pamir–Karakoram–Himalaya, The Cryosphere, 9, 557–564, https://doi.org/10.5194/tc-9-557-2015, 2015.

Kamniansky, G. and Pertziger, F.: Optimization of mountain glacier mass balance measurements, Zeitschrift für Gletscherkunde und Glazialgeologie, 32, 167–75, 1996.

Kaser, G., Großhauser, M., and Marzeion, B.: Contribution potential of glaciers to water availability in different climate regimes, P. Natl. Acad. Sci. USA, 107, 20223–20227, https://doi.org/10.1073/pnas.1008162107, 2010.

Kenzhebaev, R., Barandun, M., Kronenberg, M., Chen, Y., Usubaliev, R., and Hoelzle, M.: Mass balance observations and reconstruction for Batysh Sook Glacier, Tien Shan, from 2004 to 2016, Cold Reg. Sci. Tech., 135, 76–89, 2017.

Korona, J., Berthier, E., Bernard, M., Rémy, F., and Thouvenot, E.: SPIRIT. SPOT 5 stereoscopic survey of polar ice: reference images and topographies during the fourth International Polar Year (2007–2009), ISPRS J. Photogramm., 64, 204–212, https://doi.org/10.1016/j.isprsjprs.2008.10.005, 2009.

Kronenberg, M., Barandun, M., Hoelzle, M., Huss, M., Farinotti, D., Azisov, E., Usubaliev, R., Gafurov, A., Petrakov, D., and Kääb, A.: Mass-balance reconstruction for Glacier No. 354, Tien Shan, from 2003 to 2014, Ann. Glaciol., 57, 92–102, https://doi.org/10.3189/2016AoG71A032, 2016.

Kulkarni, A. V.: Mass balance of Himalayan glaciers using AAR and ELA methods, J. Glaciol., 38, 101–104, https://doi.org/10.3189/S0022143000009631, 1992.

Kulkarni, A. V.: Monitoring Himalayan cryosphere using remote sensing techniques, J. Indian I. Sci., 90, 457–469, 2012.

Kulkarni, A. V., Rathore, B., and Alex, S.: Monitoring of glacial mass balance in the Baspa basin using accumulation area ratio method, Current Science, 86, 185–190, 2004.

Kulkarni, A. V., Rathore, B., Singh, S., and Bahuguna, I.: Understanding changes in the Himalayan cryosphere using remote sensing techniques, Int. J. Remote Sens., 32, 601–615, https://doi.org/10.1080/01431161.2010.517802, 2011.

LaChapelle, E.: Assessing glacier mass budgets by reconnaissance aerial photography, J. Glaciol., 4, 290–297, 1962.

Liu, Q. and Liu, S.: Response of glacier mass balance to climate change in the Tianshan Mountains during the second half of the twentieth century, Clim. Dynam., 46, 303–316, https://doi.org/10.1007/s00382-015-2585-2, 2016.

Lliboutry, L.: Traité de glaciologie: Glaciers, Variations du climat, Sols gelés, vol. 2, Masson, 1965.

Marti, R., Gascoin, S., Berthier, E., de Pinel, M., Houet, T., and Laffly, D.: Mapping snow depth in open alpine terrain from stereo satellite imagery, The Cryosphere, 10, 1361–1380, https://doi.org/10.5194/tc-10-1361-2016, 2016.

Mernild, S. H., Pelto, M., Malmros, J. K., Yde, J. C., Knudsen, N. T., and Hanna, E.: Identification of snow ablation rate, ELA, AAR and net mass balance using transient snowline variations on two Arctic glaciers, J. Glaciol., 59, 649–659, https://doi.org/10.3189/2013JoG12J221, 2013.

Munia, H., Guillaume, J., Mirumachi, N., Porkka, M., Wada, Y., and Kummu, M.: Water stress in global transboundary river basins: significance of upstream water use on downstream stress, Environ. Res. Lett., 11, 014002, https://doi.org/10.1088/1748-9326/11/1/014002, 2016.

Nuth, C. and Kääb, A.: Co-registration and bias corrections of satellite elevation data sets for quantifying glacier thickness change, The Cryosphere, 5, 271–290, https://doi.org/10.5194/tc-5-271-2011, 2011.

Østrem, G.: The transient snowline and glacier mass balance in southern British Columbia and Alberta, Canada, Geogr. Ann. A., 55, 93–106, 1973.

Østrem, G.: ERTS data in glaciology – an effort to monitor glacier mass balance from satellite imagery, J. Glaciol., 15, 403–415, 1975.

Paul, F., Barrand, N., Baumann, S., Berthier, E., Bolch, T., Casey, K., Frey, H., Joshi, S., Konovalov, V., Le Bris, R., Mölg, N., Nosenko, G., Nuth, C., Pope, A., Racoviteanu, A., Rastner, P., Raup, B.. Scharrer, K., Steffen, S., and Winsvold, S.: On the accuracy of glacier outlines derived from remote-sensing data, Ann. Glaciol., 54, 171–182, https://doi.org/10.3189/2013AoG63A296, 2013.

Paul, F., Bolch, T., Kääb, A., Nagler, T., Nuth, C., Scharrer, K., Shepherd, A., Strozzi, T., Ticconi, F., Bhambri, R., Berthier, E., Bevan, S., Gourmelen, N., Heid, T., Jeong, S., Kunz, M., Lauknes, T. R., Luckman, A., Merryman Boncori, J. P., Moholdt, G., Muir, A., Neelmeijer, J., Rankl, M., VanLooy, J., and Van Niel, T.: The glaciers climate change initiative: Methods for creating glacier area, elevation change and velocity products, Remote Sensing of Environment, 162, 408–426, https://doi.org/10.1016/j.rse.2013.07.043, 2015.

Pelto, M.: Satellite identification of transient snowline variation during the melt season for mass balance assessment Taku and Brady Glacier, Alaska, in: 67th Eastern Snow Conference (ESC),

Jiminy Peak Mountain Resort, Hancock, MA, USA, 8–10 June 2010, 51–60, 2010.

Pelto, M., Kavanaugh, J., and McNeil, C.: Juneau Icefield Mass Balance Program 1946–2011, Earth Syst. Sci. Data, 5, 319–330, https://doi.org/10.5194/essd-5-319-2013, 2013.

Pertziger, F.: Abramov Glacier data reference book: climate, runoff, mass balance, Central Asian Regional Research Hydrometeorological Institute, Tashkent, Republic of Uzbekistan, 279 pp., 1996.

Pieczonka, T. and Bolch, T.: Region-wide glacier mass budgets and area changes for the Central Tien Shan between 1975 and 1999 using Hexagon KH-9 imagery, Global Planet. Change, 128, 1–13, https://doi.org/10.1016/j.gloplacha.2014.11.014, 2015.

Pieczonka, T., Bolch, T., Junfeng, W., and Shiyin, L.: Heterogeneous mass loss of glaciers in the Aksu-Tarim Catchment (Central Tien Shan) revealed by 1976 KH-9 Hexagon and 2009 SPOT-5 stereo imagery, Remote Sens. Environ., 130, 233–244, https://doi.org/10.1016/j.rse.2012.11.020, 2013.

Pohl, E., Gloaguen, R., Andermann, C., and Knoche, M.: Glacier melt buffers river runoff in the Pamir Mountains, Water Resour. Res., 53, 2467–2489, 2017.

Rabatel, A., Dedieu, J.-P., and Vincent, C.: Using remote-sensing data to determine equilibrium-line altitude and mass-balance time series: validation on three French glaciers, 1994–2002, J. Glaciol., 51, 539–546, https://doi.org/10.3189/172756505781829106, 2005.

Rabatel, A., Dedieu, J.-P., Thibert, E., Letreguilly, A., and Vincent, C.: 25 years (1981–2005) of equilibrium-line altitude and mass-balance reconstruction on Glacier Blanc, French Alps, using remote-sensing methods and meteorological data, J. Glaciol., 54, 307–314, https://doi.org/10.3189/002214308784886063, 2008.

Rabatel, A., Bermejo, A., Loarte, E., Soruco, A., Gomez, J., Leonardini, G., Vincent, C., and Sicart, J. E.: Can the snowline be used as an indicator of the equilibrium line and mass balance for glaciers in the outer tropics?, J. Glaciol., 58, 1027–1036, https://doi.org/10.3189/2012JoG12J027, 2012.

Rabatel, A., Letréguilly, A., Dedieu, J.-P., and Eckert, N.: Changes in glacier equilibrium-line altitude in the western Alps from 1984 to 2010: evaluation by remote sensing and modeling of the morpho-topographic and climate controls, The Cryosphere, 7, 1455–1471, https://doi.org/10.5194/tc-7-1455-2013, 2013.

Rabatel, A., Dedieu, J. P., and Vincent, C.: Spatio-temporal changes in glacier-wide mass balance quantified by optical remote sensing on 30 glaciers in the French Alps for the period 1983–2014, J. Glaciol., 62, 1153–1166, https://doi.org/10.1017/jog.2016.113, 2016.

Rabatel, A., Sirguey, P., Drolon, V., Maisongrande, P., Arnaud, Y., Berthier, E., Davaze, L., Dedieu, J.-P., and Dumont, M.: Annual and Seasonal Glacier-Wide Surface Mass Balance Quantified from Changes in Glacier Surface State: A Review on Existing Methods Using Optical Satellite Imagery, Remote Sens., 9, 507, https://doi.org/10.3390/rs9050507, 2017.

Schaner, N., Voisin, N., Nijssen, B., and Lettenmaier, D. P.: The contribution of glacier melt to streamflow, Environ. Res. Lett., 7, 034029, https://doi.org/10.1088/1748-9326/7/3/034029, 2012.

Sevruk, B.: Methodische Untersuchungen des systematischen Messfehlers der Hellmann-Regenmesser im Sommerhalbjahr in der Schweiz (Methodical investigations of the systematic error of the Hellmann raingauge in the summer season in the Switzerland), PhD thesis, Versuchsanstalt für Wasserbau, Hydrologie und Glaziologie, ETH Zürich, Mitt. 52, 296 pp., 1981.

Shea, J. M., Immerzeel, W. W., Wagnon, P., Vincent, C., and Bajracharya, S.: Modelling glacier change in the Everest region, Nepal Himalaya, The Cryosphere, 9, 1105–1128, https://doi.org/10.5194/tc-9-1105-2015, 2015.

Shean, D. E., Alexandrov, O., Moratto, Z. M., Smith, B. E., Joughin, I. R., Porter, C., and Morin, P.: An automated, open-source pipeline for mass production of digital elevation models (DEMs) from very-high-resolution commercial stereo satellite imagery, ISPRS J. Photogramm., 116, 101–117, https://doi.org/10.1016/j.isprsjprs.2016.03.012, 2016.

Sorg, A., Bolch, T., Stoffel, M., Solomina, O., and Beniston, M.: Climate change impacts on glaciers and runoff in Tien Shan (Central Asia), Nat. Clim. Change, 2, 725–731, https://doi.org/10.1038/nclimate1592, 2012.

Stocker, T. F., Qin, D., Plattner, G.-K., Tignor, M., Allen, S. K., Boschung, J., Nauels, A., Xia, Y., Bex, B., and Midgley, B.: IPCC, 2013: climate change 2013: the physical science basis. Contribution of working group I to the fifth assessment report of the intergovernmental panel on climate change, New York, NY, USA, Cambridge University Press, 1535 pp. 2013.

Suslov, B., Akbarov, A., and Yemelyanov, J.: Abramov glacier, Hydrometeoizdat, Leningrad, 1980.

Unger-Shayesteh, K., Vorogushyn, S., Farinotti, D., Gafurov, A., Duethmann, D., Mandychev, A., and Merz, B.: What do we know about past changes in the water cycle of Central Asian headwaters? A review, Global Planet. Change, 110, 4–25, https://doi.org/10.1016/j.gloplacha.2013.02.004, 2013.

Varis, O.: Curb vast water use in central Asia, Nature, 514, 27–30, https://doi.org/10.1038/514027a, 2014.

Wang, Q., Yi, S., Chang, L., and Sun, W.: Large-scale seasonal changes in glacier thickness across High Mountain Asia, Geophys. Res. Lett., 44, 10427–10435, https://doi.org/10.1002/2017GL075300, 2017.

WGMS: Glacier Mass Balance Bulletin No. 12 (2010–2011), edited by: Zemp, M., Nussbaumer, S. U., Naegeli, K., Gärtner-Roer, I., Paul, F., Hoelzle, M., and Haeberli, W., ICSU (WDS) / IUGG (IACS) / UNEP / UNESCO / WMO, World Glacier Monitoring Service, Zurich, Switzerland, 106 pp., https://doi.org/10.5904/wgms-fog-2013-11, 2013.

Wu, L., Li, H., and Wang, L.: Application of a degree-day model for determination of mass balance of Urumqi Glacier No. 1, eastern Tianshan, China, J. Earth Sci., 22, 470–481, https://doi.org/10.1007/s12583-011-0201-x, 2011.

Wu, Y., He, J., Guo, Z., and Chen, A.: Limitations in identifying the equilibrium-line altitude from the optical remote-sensing derived snowline in the Tien Shan, China, J. Glaciol., 60, 1093-1-100, https://doi.org/10.3189/2014JoG13J221, 2014.

Young, G. J.: The mass balance of Peyto glacier, Alberta, Canada, 1965 to 1978, Arctic Alpine Res., 13, 307–318, 1981.

Zhang, Y., Liu, S., Xie, C., and Ding, Y.: Application of a degree-day model for the determination of contributions to glacier meltwater and runoff near Keqicar Baqi glacier, southwestern Tien Shan, Ann. Glaciol., 43, 280–284, https://doi.org/10.3189/172756406781812320, 2006.